Characterizing four decades of accelerated glacial mass loss in the West Nyainqentanglha Range of the Tibetan Plateau

Shuhong Wang[1,2,3], Jintao Liu[1,2*], Hamish D. Pritchard [3], Linghong Ke[2], Xiao Qiao[1,2], Jie Zhang[1,2], Weihua Xiao[4], Yuyan Zhou[4]

[1]State Key Laboratory of Hydrology-Water Resources and Hydraulic Engineering, Hohai University, Nanjing 210098, People's Republic of China.

[2]College of Hydrology and Water Resources, Hohai University, Nanjing 210098, People's Republic of China.

[3]British Antarctic Survey, Cambridge, CB3 0ET, UK.

[4]State Key Laboratory of Simulation and Regulation of Water Cycle in River Basin, China Institute of Water Resources and Hydropower Research, Beijing 100038, China.

* *Correspondence:* jtliu@hhu.edu.cn; Tel.: +86-025-83787803

Abstract:

Glacier retreat is altering the water regime of the Tibetan Plateau (TP) as the region's climate changes, but there remain substantial gaps in our knowledge of recent glacier loss in this region due to the difficulty of making- direct high-mountain observations and this limits our ability to predict the future of this important water resource. Here, we assessed 44 years of glacier area and volume changes in the major West Nyainqentanglha Range (WNR) that supplies meltwater to the densely populated Lhasa River basin and Nam Co, the second largest endorheic lake on the TP. Between the two periods 1976-2000 and 2000-2020, we found that the glacier areal retreat rate was more than doubled (from -0.54 ± 0.21 % a^{-1} to -1.17 ± 0.30 % a^{-1}) and surface lowering also accelerated (from -0.26 ± 0.09 m w.e.a^{-1} to -0.37 ± 0.15 m w.e.a^{-1}) with particularly intense melting after 2014. This acceleration is similar in both timing and magnitude to that observed for Himalayas glaciers farther south. Besides, the areal retreat rate and mass loss rate of most glaciers in WNR were not synchronized. To understand the sensitivity of WNR glaciers to climate forcing, we examined the effects of topography, debris-cover, and the presence of proglacial lakes on our observed changes. We found consistently faster areal retreat but slower thinning rates on steeper slopes and an inconsistent relationship with aspect. We concluded that our observed spatial and temporal patterns of glacier change were dominated by observed local variations temperature and precipitation, the melt-reducing role of supraglacial debris, and the increasing influence of ice-marginal lakes on glacier retreat.

1. Introduction

The Tibetan Plateau (TP) known as the "Water Tower of Asia", is the source of several of Asia's major rivers (Bolch et al., 2010) and glacial melt on the TP plays an important role in water supply for downstream populations, agriculture and industries along these rivers (Pritchard, 2019; Viviroli et al., 2007). Climate change over recent decades has boosted river discharge by increasing runoff from shrinking glaciers (Lin et al., 2020; Yao et al., 2007; Zhang et al., 2011a), but this boost

will eventually decrease as glacier area declines (Zhao et al., 2019). The sensitivity of ice loss to climate change is variable, however, and often poorly known, being a function of glacier size, hypsometry, aspect, debris cover, and the presence of proglacial lakes and ice cliffs, for example. Combined with uncertainties in ice thickness and future climate scenarios, the timing of peak water runoff and the rate of its subsequent decline remain key unknows (Maurer et al., 2019; Nie et al.,2021; Su et al., 2016; Zhao et al., 2019). It is therefore critical to monitor and analyze glacier change to improve our understanding of its climate drivers, and to assess its impacts on glacier-fed river basins.

Compared with the interpolation of sparse in-situ measurements, satellites can observe glacier change over much larger areas of remote terrain (Wang et al., 2021a). In recent years, our understanding of the state of TP glaciers has been greatly improved by the increasing coverage and accuracy of multi-source remote sensing observations of glacier area, volume and mass change from KH-9 (Hexagon military satellites), Landsat, ASTER, ICESat altimetry, and other Digital Elevation Models (DEMs) constructed by geodetic techniques, and from GRACE gravimetry (Guo et al., 2015; Kääb et al., 2012; Wang et al., 2021a; Zhou et al., 2018). Based on the KH-9 images and SRTM, for example, Zhou et al. (2018) found that from the mid-1970s to 2000 glaciers in the northwest TP thinned at -0.11 ± 0.13 m w.e. a^{-1} to 0.02 ± 0.10 m w.e. a^{-1} while those in the southeast part thinned faster at -0.30 ± 0.12m w.e. a^{-1} to -0.11 ± 0.14m w.e. a^{-1}. Brun et al. (2018a) employed ASTER DEMs from 2000-2006 and showed that glacier mass balance in High Mountain Asia varied from -0.62 ± 0.23 m w.e. a^{-1} in eastern Nyainqentanglha to $+0.14 \pm 0.08$ m w.e. a^{-1} in the Kunlun Mountains, and averaged -0.14 ± 0.14 m w.e. a^{-1} over the large Inner TP that includes WNR. Maurer et al. (2019) found a doubling of the Himalayan average loss rate between the periods 1976-2000 (-0.22 ± 0.13 m w.e. a^{-1}) and during 2000–2016 (-0.43 ± 0.14 m w.e. a^{-1}) using KH-9 and ASTER DEMs. These studies showed that glacier changes on and around the TP have marked spatial and temporal heterogeneity, likely associated in part with variable glacial sensitivity to climate change (Yao et al., 2012).

The drivers of regional glacier loss include, for example, a jump in mean annual temperature and precipitation in the Yarlung-Zangpo River basin around 1997 (Wang et al., 2021b) and an accelerating warming trend over the TP between the periods 1980–1997 and 1998–2013 (from 0.21 °C to 0.25 °C decade^{-1}) (Duan & Xiao, 2015).Modulating the effect of these climatic drivers are local factors including glacier topography, debris-cover and, glacial lakes (Brun et al., 2018b, 2019; Ke et al., 2020; Maurer et al., 2019; Pandey et al., 2017; Yao et al., 2012). Some studies have analyzed the melt-inhibiting effect of debris cover and melt-promoting effect of proglacial lakes on glacier ablation since 2000 (Ke et al., 2020; Vincent et al., 2016), but with the potential for KH-9 in 1976, SRTM in 2000, ASTER in 2000-2020 and aerial mapping Landsat 1976-2020 through time, we are now able to assess glacier area and mass change in the WNR in relation to both regional climatic derivers and local modulating factors.

The WNR, in the south-eastern TP (Figure 1), is located in the transition zone between the two large-scale atmospheric circulation patterns characterized respectively by dominant westerlies and the Indian summer monsoon. It holds an abundance of glaciers and glacial-fed lakes, notably Nam Co Lake (Figure 1), whose rising water levels indicate a water imbalance

primarily due to recently intensified glacier melting (Bolch et al., 2010), as supported by mass balance data from Zhadang

Glacier and other hydrological observations from 2007 to 2011 (Zhou et al., 2013). The number and area of supraglacial lakes

(of >0.0036 km^2) in the WNR also increased between 1976 and 2018 by 56% and 35% respectively due to the increase in

glacial meltwater (Luo et al., 2020). In the relatively densely-populated Lhasa Basin to the southeast of WNR, Lin et al. (2020)

found that a water imbalance also existed using the first and second Chinese Glacier Inventory in 1960 and 2009. Despite these

extensive changes and large affected population, logistical constraints have meant that in situ glacier mass balance records are

limited to a few low-lying, small glaciers that are unlikely to be representative of the broader region (Kääb et al., 2012; Li &

Lin, 2017; Yao et al., 2012).Similarly, glacier volumes in the Chinese Glacier Inventory were primarily calculated indirectly

by area-volume scaling, and limited direct observations mean that these volume have larger uncertainty (Bahr et al., 1997;

Bahr et al., 2015). Detailed investigation of the WNR glacier area change and mass balance on a longer time scale is therefore

a high priority.

 Investigations of WNR glacier area have so far focused on the period before 2014 (Bolch et al., 2010; Wu et al., 2016).

For glacier mass balance, most studies focus on after 2000 (Li & Lin, 2017; Neckel et al., 2014; Ren et al., 2020; Zhang &

Zhang, 2017). There are limited discussions on local glacier changes in the WNR region from before 2000, although Zhou et

al. (2018) included this area in his study of glacier mass balance on the TP and its surroundings from the mid-1970s to 2000

and did not present the characteristics of glacier changes in detail. Furthermore, the warming rate of the TP is heterogeneous

both spatially and temporally in recent decades (Duan & Xiao, 2015; Wu et al., 2015). Under a changing runoff regime (Lin

et al., 2020), the lack of a detailed survey of glacier changes over a long time scale is a major impediment to water resource

management and decision-making (Lutz et al., 2014).

 The key purpose of this study is therefore to provide an internally consistent dataset of glacier area and mass change in

the WNR over the past 44 years, and comparative analysis of the impact of topography, debris and proglacial lakes on glacier

change during 1976 - 2000 and during 2000 - 2020. Although the area of both debris-cover and lake terminating glaciers are

relatively small, the characteristics of their influence on individual glaciers can be used as a reference for glacier changes in

other regions. We have compiled a complete glacier inventory in the years 1976, 2000, 2014 and 2020 with the Landsat and

KH-9 images and quantified the geodetic glacier mass balance during 1976–2000 and 2000–2020 with DEMs derived from

KH-9, ASTER and SRTM3.0. We report area and mass changes for periods 1976 to 2000 and from 2000 to 2020, and we

examine and compare the influence of topographic, climatic, and glaciological factors on these changes during 1976-2000 and

2000-2020.

2. Materials and methods

2.1 Study area

 The WNR has a mean slope of 15° and its elevation spanning 4150-7125 m, with an average of 4930 m in the whole

region. Its primary mountain ridge runs 230 km in a southwest−northeast direction, bounded by the Nam Co basin to the north and the Lhasa River basin to the south (Yao et al., 2010). Nam Co Lake, the second largest after Selin Co Lake on the TP, is mainly fed by glacier meltwater (Luo et al., 2020; Zhang et al., 2017). The Lhasa River basin to the southeast is a major branch of the Yarlung Zangbo River and forms part of the route taken by the warm and humid monsoon airflow into the plateau, making it warmer and wetter than the Nam Co basin (Luo et al., 2020). The annual air temperature and precipitation in the WNR range from −0.6℃ to 2.8℃ and 37 mm to 500 mm, respectively (Yu et al., 2013).

Being in a climatic transition zone, the glaciers in this area range from the maritime-influenced glaciers of Gangrigabu (southeast TP) to the subcontinental and continental-type glaciers of the Tanggula mountains (Li & Lin, 2017). There are 845 glaciers covering 675.85 km^2 and 15 debris-covered glaciers with a total area of 71.74km^2 (10.61% of the total glacier area in the WNR) (RGI 6.0) (RGI Consortium, 2017). Of these, only the small, ~3km^2 Zhadang and Gurenhekou glaciers (red polygon in Figure 1) have in-situ observations available to validate the satellite observations, and these run from 2005 to 2010 (Yao et al., 2012).

2.2 Methods and data

2.2.1 Glacier outlines

We identified glacier boundaries mainly from Landsat MSS/ETM+/OLI scenes from various years (Table S1), orthorectified automatically by the USGS using the level 1T SRTM3 DEM (from http://glovis.usgs.gov/). We selected high-quality images with minimal cloud and snow coverage between June and November and used a semi-automated approach with a TM3/TM5 band ratio (2.0 ± 0.2) to produce glacier outlines. This method is widely used and appropriate for glacier mapping over large study areas (Guo et al., 2015; Ye et al., 2017). We used a 3 × 3 median filter to eliminate isolated pixels and likely to have been misclassified due to debris or boulders on the glacier (Bolch et al., 2010). We manually checked and edited the glacier outlines, including the debris-covered glaciers, with height change maps and a coherence map formed by Sentinel-1 images observed on 2016-08-05 and 2016-08-29, to help distinguish debris-covered ice from ice-free areas. Finally, referring to the second glacier inventory, we assigned contiguous ice masses to drainage basins in order to obtain a glacier inventory.

2.2.2 Glacier elevation change

We used the KH-9 images and SRTM DEM (version 3) to estimate glacial elevation changes for the period 1976 to 2000, and ASTER DEMs for the period 2000-2020.

2.2.2.1 DEM data

The declassified KH-9 images were obtained by the Hexagon mission from 1971 to 1986, with a ground resolution of 6 to 9 m (Surazakov & Aizen, 2010). We downloaded images from 1976-01-07 via the Earth Explorer user interface (https://earthexplorer.usgs.gov) and adopted the Hexagon Imagery Automated Pipeline method to generate digital elevation

125 models. This method is coded in MATLAB and uses the OpenCV library for Oriented FAST and Rotated BRIEF (ORB) feature

126 matching, uncalibrated stereo rectification, and semiglobal block matching algorithms (Maurer & Rupper, 2015).

127 The SRTM mission carried out in February 2000 produced two types of DEM datasets, the C-band DEM with a coverage

128 range of 60°N ~ 60°S and the X- band DEM with a smaller coverage. We used version 3 of the C-band SRTM DEM

129 (https://earthexplorer.usgs.gov/) at 1-arc-second resolution (about 30 m) in our primary processing and masked out areas with

130 gaps in the unfilled SRTM3 version 2.1 DEM at 3-arcsencond resolution (about 90 m).

131 The ASTER instrument was launched on the Terra satellite in December 1999 and a single DEM covers approximately

132 3600 km^2. We downloaded 250 'Data1. l3a.demzs' ASTER DEMs at 30 m resolution in geotiff format with cloud coverage of

133 less than 40% from the METI AIST Data Archive System (MADAS) satellite data retrieval system (https://gbank.gsj.jp/madas).

134 After cloud and outlier removal we fitted a linear regression through the time series of co-registered ASTER DEMs and set

135 the minimum stack interval per pixel to 15 years to estimate the rate of elevation change for each 30-m pixel (Maurer et al.,

136 2019).

137 2.2.2.2. Co-registration and bias correction of DEMs

138 All DEMs were co-registered to the SRTM master DEM using a standard elevation–aspect optimization procedure (Nuth

139 & Kääb, 2011). Then, the elevation correlation deviation of all the DEMs was corrected by a third-order polynomial. In addition,

140 we used a 2km buffer zone around the union of glacier boundaries to define stable (unchanging) terrain for DEM alignment,

141 bias correction, and uncertainty calculation. Figure. S1a shows the coverage of the KH-9 images and the number of valid

142 ASTER DEMs grids after removal of clouds and outliers in the buffer. The glacier area covered by the dataset from 1976 to

143 2000 and from 2000 to 2020 accounted for 70.85% and 81.94% of the total glacier area, respectively (shown in Figure. S1b,

144 c). We used only the area common to both of these datasets to measure elevation change between the 1976-2000 and 2000-

145 2020 periods. After correction for alignment and elevation-related deviation, apparent elevation changes over stable terrain

146 (masked glaciers and lakes in square buffer zone) had no change trend with elevation, slope and aspect, as shown in Figure.

147 S2.

148 2.2.2.3. SRTM Penetration depth correction

149 Over the WNR, the average penetration depth of C-band SRTM is 1.67 ± 0.53 m calculated using X- band SRTM DEM

150 as the reference (Li & Lin, 2017). Linear regression between the glacier elevation and penetration showed that the penetration

151 depth varies from 1.29 m to 2 m at altitudes of 5550 m and 6250m respectively (Li & Lin, 2017). We used this more accurate

152 linear altitude-dependent correction, and the result is similar to several other study regions on the TP (Gardelle et al., 2013;

153 Kääb et al., 2012; Li & Lin, 2017).

154 2.2.2.4 Glacier mass change

155 Estimation of average glacier thickness changes based on elevation difference maps involves noise filtering and glacier-

156 hypsometry-weighted averages in an approach widely employed in to calculate regional glacier mass balance where glacier

157 thinning is highly dependent on altitude. Firstly, we subjected the thickness change maps to outlier removal using a 5 m a^{-1}

158 threshold. We then masked slopes > 45°, where uncertainties are large, before visually inspecting the final thickness change

159 maps. We additionally masked out any remaining anomalous pixels, which occurred almost exclusively in low-contrast, snow-

160 covered accumulation zones. Finally, we separated thickness changes into 50-m elevation bins by referring to the SRTM at

161 different spatial scales, i.e., the whole glacierized area, sub-regions, different glacier types and individual glaciers of area >2

162 km^2. In each altitude bin, we filtered out any height-change values that differed by more than three standard deviations from

163 the median and removed any bins with less than 100 pixels. For elevation bins with no observations (mostly over the low- and

164 high- elevation limits), we assumed zero mean elevation changes. We calculated the mean glacier thickness changes for the

165 spatial unit/group (dh) as a hypsometric average:

$$dh = \sum_{i=1}^{n} \frac{S_i}{S} \cdot \overline{dh_i} \qquad (1)$$

167 where i and n denote the ith 50-m elevation bin and the number of total bins respectively, S_i is the glacier area of the ith elevation

168 bin, S is the total glacier area, and $\overline{dh_i}$ is the mean dh in the bin.

169 We calculated the final geodetic mass balance (B) using equation (2).

$$B = dh_i \times \frac{\rho_{ice}}{\rho_{water}} \qquad (2)$$

171 We translated glacier thickness changes into mass balance by the ratio of column-averaged glacier density, ρ_{ice} (850 kg m^{-3}) to

172 water density (ρ_{water}, 1000 kg m^{-3}).

2.2.3 Uncertainty

174 2.2.3.1 Uncertainty of glacier area

175 Similar to previous studies (Wu et al., 2016; Ye et al., 2017), we obtained the uncertainty of glacier area (δ_s) using equation

176 (3).

$$\delta_s = L_c E_{pc} + L_d E_{pd} \qquad (3)$$

178 Where L_c and L_d represent the lengths of the clean-ice and debris-covered glacier outlines, and E_{pc} and E_{pd} denote the positional

179 accuracies. We calculated the uncertainty in glacier area change (δ_{sc}) by combining the area uncertainties using equation (4).

$$\delta_{sc} = \sqrt{(\delta_{s1})^2 + (\delta_{s2})^2} \qquad (4)$$

181 Guo et al. (2015) compared glacier outlines derived from Landsat-images with real-time kinematic differential GPS (RTK-

182 DGPS) measurements and found an average difference of ±11 m and ±30 m for the delineation of clean and debris-covered

183 ice. Using a buffer size of 10 m for areas from the Hexagon images (Bolch et al., 2010), our combined uncertainty in glacier

184 area is 3.9%, 5.1%, 5.1% and 5.9% in 1976, 2000, 2014, and 2020, respectively.

185   2.2.3.2 Uncertainty of glacier thickness change

186   The uncertainty in surface-elevation change derived from ASTER DEMs can be estimated using the point elevation error

187   (E_{pt}) and extrapolation error (E_{ext}) (Nuth & Kääb, 2011; Maurer et al., 2016).

188
$$\delta_{hi} = \sqrt{(\frac{E_{pt}}{\sqrt{n_i}})^2 + (\frac{E_{ext}}{\sqrt{n_i}})^2} \qquad (5)$$

189
$$n_i = \frac{n_{ib} * r^2}{\pi * d^2} \qquad (6)$$

190
$$\delta_h = \sqrt{\sum_{i=1}^{i=n}(\delta_{hi} * \frac{S_i}{S})^2} \qquad (7)$$

191   Here, E_{pt} refers to the standard deviations of the relative elevation change over the off- glacier areas, E_{ext} is the standard

192   deviations of glacial elevation change within each 50-m bin, n_{ib} and n_i represent the total number of pixels and the number of

193   independent measurements of pixels respectively, r is the DEM spatial resolution (30 m in our study), and d is the

194   autocorrelation length. We used an autocorrelation length of 500 m was employed, which is a conservative value based on

195   semivariogram analysis of mountainous regions in previous studies (Brun et al., 2018a; Maurer et al., 2019). We combined,

196   the uncertainty of surface-elevation changes derived from the KH-9 DEM with the SRTM penetration uncertainty, estimated

197   as ±0.53 m (Li & Lin, 2017). This study ignored the errors caused by seasonal changes in glacier thickness due to the lack of

198   observations of such seasonal changes.

199   We estimated the overall uncertainty in the total glacier mass change (δm, in kg) by including the uncertainty in the

200   assumed ice/firn/snow density ($\delta\rho$ = 60 kg m^{-3}, which is 7.1% of ρ_{ice} = 850 kg m^{-3}), errors in glacier area (δ_S, m^2) and glacier

201   elevation change (δ_h, m), using equation (8).

202
$$\delta_m = \sqrt{(S \cdot dh \cdot \delta_\rho)^2 + (\delta_s \cdot dh \cdot \rho_{ice})^2 + (S \cdot \delta_h \cdot \rho_{ice})^2} \qquad (8)$$

203 **2.2.4. Lake data**

204   We identified glacier-marginal lakes as those lying within 50 m of a glacier boundary, using lake data for the 1970s-2018

205   (Luo et al., 2020; http://data.tpdc.ac.cn).

206 **2.2.5. Meteorological data**

207   There are three meteorological stations adjacent to the WNR, at Bange (31°23′N, 90°01′E, elevation of 4700 m), Lhasa

208   (29°40′N, 91°08′E, elevation of 3648 m), and Damxung (30°29′N, 91°06′E, elevation of 4200 m). We obtained air temperature

209   and precipitation data during 1976-2020 from the Climatic Data Center, National Meteorological Information Center, of the

210   China Meteorological Administration.

211   We also obtained gridded data of precipitation and temperature with spatial resolution of 0.1° × 0.1° and 3-h time interval

212 for 1979-2018 from the China Meteorological Forcing Data (Ding et al., 2020; http://data.tpdc.ac.cn), which has been widely

213 utilized in land-process, hydrological modelling, and other studies (Qiao et al., 2021; Wang et al., 2021b). This dataset is made

214 by fusing the conventional meteorological observation of China Meteorological Administration based on the Princeton

215 reanalysis data, GLDAS data, GEWEX-SRB radiation data, and TRMM precipitation data as the background field(He et al.,

216 2020; Yang et al., 2010).

217 **2.2.6 Hydrological Data**

218 In order to assess hydrological changes under glacier retreat, we have collected runoff data of the Lhasa River station
219 during 1976-2013 and the Yangbajain station during 1979-2013 from the Tibet Autonomous Region Hydrology and Water
220 Resources Survey Bureau.

221 We calculated the ratio of total glacier mass change to runoff in Lhasa River basin (R_r, %) and the total lake water
222 storage change of Nam Co Lake (R_l, %) as follows:

223
$$R_r = \frac{\Delta M * S_g}{S_r R_a} \qquad (9)$$

224
$$R_l = \frac{\Delta M * S_g}{\Delta V} \qquad (10)$$

225 Where ΔM, S_g, S_r, R_a, ΔV represent average annual glacier mass balance, glacier area, area of the Lhasa River basin,
226 average runoff depth, lake water storage increase.

227 **3.Results**

228 **3.1 Glacier area change**

229 There were 921 glaciers with a total area of 589.17 ± 31.72 km^2 in 2020 in the WNR (Figure 2a). Small glaciers dominated

230 the number (those ≤ 1 km^2 occupy 83.17% of the total number) and a large proportion of the area (those ≤ 1 km^2 occupy 30.42%

231 of the total area). Glaciers larger than 5 km^2 accounted for 21.39% of the total area and only 1.63% of the total number. Glaciers

232 were mainly distributed in the eastern-oriented zone with an altitude of 5600-6100m and a slope of 5-40° (Figure 2b, c, d).

233 Glaciers in the WNR experienced significant retreat from 1976 to 2020 and altitude, slope and aspect all appear to have

234 influenced this retreat (Figures 3 and 4). The glacier area decreased from 884.90 ± 29.71 km^2 in 1976 to 589.17 ± 31.72 km^2

235 in 2020, with an average annual decrease of -0.76 ± 0.11 % a^{-1}. The retreat rate of glacier area in 2000-2020 (-1.17% a^{-1}) was

236 more than twice as fast as in 1976-2000 (-0.54 ± 0.21 % a^{-1}) (Figures 3 and 4, Table 1). The glacier area declined faster in the

237 northeast and southwest but slower in the middle, except for a few small glaciers with an area of less than 2 km^2 during 1976-

238 2000. During 2000-2020 the glacier area receded faster in the whole region except for a few small glaciers with an area of less

239 than 1 km^2 (Figure 3). Retreat was greatest in the area classes of 1-3 km^2 and 3-5 km^2, and glaciers with significant areal retreat

240 were mainly distributed below 6,000 m altitude. Glaciers in the Nam Co basin retreated slightly faster than those outside this

basin between 2000 and 2020. Retreat was particularly rapid at lower altitudes and decreased at higher elevations. As for the effect of slope and aspect, glacier retreated more rapidly with increasing slope between 5° and 40°, but the retreat rate decreased as slope increased between 0°-5° and 40°-60°, where relative few glaciers are distributed. In each elevation band, we found a positive correlation between areal retreat rates and slope (faster retreat with steeper slope) for most elevation bands and in both time periods (Figure 9 a and b). The only areas where this relationship differed were on flat or shallow slopes at lower altitudes (slopes below about 5° at elevations below about 5500 m, e.g., blue lines in Figure 9a) which also experienced relatively rapid retreat. During both 1976-2000 and 2000-2020, the retreat rate was smallest on the north-facing slopes. During 1976-2000, retreat was most rapid in the southeast quadrant, while from 2000 to 2020, rapid retreat occurred at similar rates in all aspects other than north and southeast, i.e., the effect of aspect on glacier area retreat varied in space and time.

Besides, we noticed that the area decreased but glacier number increased in WNR (Figure 2a). The reason for this is that intact glaciers break down into several smaller glaciers in the process of glacier ablation, e g., a large glacier in 1976 may become several smaller glaciers in 2020 (shown in Figure S3).

3.2 Geodetic mass balance

Glacier height changes for the past 44 years, are shown in Figure 5. Substantial and near-ubiquitous thinning occurred in the WNR during 1976-2020 (with mean surface lowering of -0.37 ±0.13 m a^{-1}, a water-equivalent loss rate of -0.31 ± 0.12 m w.e. a^{-1} or a mass loss rate of -0.26 ± 0.09 Gt a^{-1}), with a widespread increase in the most recent decades. From 1976 to 2000, glaciers experienced a mean thinning rate of -0.31 ± 0.10 m a^{-1} (-0.26 ± 0.09 m w.e. a^{-1}) or -0.24 ± 0.08 Gt a^{-1}. From 2000 to 2020, the mean elevation rate was -0.44 ± 0.13 m a^{-1}, (0.37 ± 0.12 m w.e. a^{-1}) or -0.29 ± 0.09 Gt a^{-1}. Several glacier tongues have suffered severe thinning, exceeding -1.5 m a^{-1} from 1976 to 2000, notably several long, debris-free glaciers on the south-western slope. From 2000 to 2020, the range of glacier tongues with losses exceeding 1.5 m a^{-1} expanded, and losses were greater in the central WNR (see, the red rectangular box in Figure 5). In both 1976-2000 and 2000-2020, the glacier thinning rate was slightly higher inside the Nam Co drainage basin than outside it (Table 2, Figure. 6), though these rates do not differ by more than their combined uncertainties.

For glaciers with an area of more than 2 km^2, we found high loss rates in the northeast, followed by the southwest, and moderate in the middle during 2000-2020, but there no obvious spatial varied trend of mass loss during 1976-2000 (Figure 7). Mass loss was substantially more intense in 2000-2020 with no glaciers in a state of positive balance (Figure 7, blue dots) and loss from some glaciers in the northeast exceeded -0.6 m w.e. a^{-1}. Moreover, we found that glacier area retreat and mass loss was not synchronized between the two periods 1976-2000 and 2000-2020. The glacier with the fastest area retreat did not correspond to the glacier with the fastest mass decrease, and the spatial varied trend of glacier area retreat rate was inconsistent with that of mass loss rate (Figure 3 and 7).

272   Finally, glacier elevation change as a function of elevation slope and aspect are shown in Figure 8. Elevation is inversely

273   correlated with thickness change, while slope and aspect appear to have a weak relationship with thickness change. In both

274   1976-2000 and 2000-2020, the elevation change rate was the largest at lower altitudes, and gradually decreased with the

275   increasing of altitude. The thinning rate also exhibited a weak inverse relationship with slope, becoming somewhat stronger in

276   the 2000-2020 period. A very similar but inverse to relationship between slope and glacier area change rate in each

277   elevation band is that thinning rates were highest on shallow slopes and decreased over steeper slopes, except for flat or

278   shallow slopes at lower altitudes where thinning rates were relatively low (Figure 9 c and d). For the impact of aspect,

279   thinning for 1976-2000 was most rapid in the south-west and north-west quadrants, but by 2000-2016 high thinning rates were

280   affecting all aspects, i.e., the effect of aspect on thinning rates also varied through time.

281   **3.3 The effect of debris-cover and proglacial lakes on glacier mass changes**

282   In our WNR study area, there are five debris-covered glaciers, covering 55.42 ± 1.25 km^2 in 1976 and 51.59 ± 1.77 km^2

283   in 2000. Lake-terminating glaciers occupied a similar proportion, with area of 70.29 ± 2.69 km^2 in 1976, and 49.60 ± 1.82 km^2

284   in 2000. Only one glacier was both covered by debris and terminated in a pro-glacial lake.

285   The thinning rate of different types of glaciers varied somewhat, though with greater uncertainty given the relatively small

286   sample. (Figure 10, Table 3). During 1976-2000, the lake-terminating glaciers thinned more rapidly, followed by the regular

287   and debris-covered glacier types. From 2000 to 2020, the ablation rate of debris-covered glaciers was slightly lower than that

288   of regular glaciers at low altitudes, but progressively greater at higher altitudes, leading to a slightly more negative total mass

289   balance for the debris-covered type. In the same period, the thinning of lake-terminating glaciers continued to exceed that of

290   regular glacier. Our results suggest that debris cover in the WNR suppressed glacier thinning to some extent and enabled the

291   debris-covered ice to survive at lower elevations than adjacent clean ice glaciers. In contrast, a glacial lake at the end of a

292   glacier accelerated its retreat, and this behavior was more pronounced at lower elevations.

293   **4.Discussion**

294   **4.1 Comparison to previous studies**

295   **4.1.1 Glacier area change**

296   Based on space-borne imagery, we found that glacier area in the west Nyainqentanglha Range (WNR) has changed by -

297   12.98±4.91 during 1976-2000 and -23.45±5.99% during 2000-2020. The comparison between this, Chinese Glacier Inventory

298   (CGI) I and CGI II over WNR, and previous studies and is shown in Tables S2 and S3. The CGI II of WNR in 2009 are in

299   good agreement with the areal retreat trend in our study (also shown in Figure 2). The CGI I of WNR in 1970 is slightly smaller

300   than the glacier area in 1976 in our study, but it is within the margin of uncertainty. The CGI I was mapped based on the

301   Chinese topographic maps, while glacier area in our study was mapped based on Landsat Images. The difference between them

might come from this difference in data source used to extract the glaciers outlines. Besides, Frauenfelder & Kääb, (2009) reported that there are georeferencing errors in the areas in GGI I. Differences between studies may have arisen from the georeferencing errors in the areas for 1970 used by Shangguan et al. (2008) and Wu & Zhu (2008) which came from the CGI I. Discrepancies may also have arisen from differences in the methods used to distinguish glaciers from seasonal snow, and debris-cover glaciers from neighboring moraine or rock slopes (Bolch et al., 2010). The deviation between our results and those from Wu et al. (2016) and Wang et al. (2012) over the whole WNT and the southwest WNT is within the margin of uncertainties. In addition, the 789.15 km^2 area reported for the WNR by RGI V4.0 which used Landsat images obtained on 2001-12-06 agrees with our result.

4.1.2 Glacier mass balance

Field measurements of mass balance are available from small Zhadang glacier for 2005-2008, and Gurenhekou glacier for 2005-2010 on the southeastern slope of the WNR (Table S4). Although the period of our study is longer and provides a much larger sample size, the mass balance results are similar to these field measurements.

Previous studies have also reported region-averaged glacier mass balance over a similar spatial extent to ours, obtained from DEMs using various sensors (Table S5). Our results during 2000-2020 are more negative than those of Neckel et al. (2014), Li & Lin (2017) and Zhang & Zhang (2017), but agree within the uncertainties over comparable time periods, even though these studies differ in data processing, glacier mask, penetration correction and data coverage. For comparison, we calculated the change for the 2000-2014 period from ASTER DEMs (Figure 11). Our estimated mass balance in this area (-0.28±0.15 m w.e. a^{-1}) is very similar to the other studies (Table S5). It is also similar to that of 1976-2000, suggesting that the more strongly negative average for the longer 2000 to 2020 period (-0.37±0.12 m w.e. a^{-1}) is mainly due to the intensified glacier ablation after 2014, although cloud-free ASTER data are insufficient for direct calculation of the mass balance from 2014-2000. The glacier area retreat during 2014-2020 (1.53±1.14 % a^{-1}) is also faster than that during 2000-2014 (1.13±0.42 % a^{-1}), though the change is within the uncertainties. This interpretation is supported by Ren et al. (2020) who also calculated a higher 2013-2020 thinning rate (-0.43±0.06 m w.e. a^{-1}) twice as negative as in 2000-2013. Though the difference in rate is within the combined uncertainties for these periods, this apparent acceleration in thinning in WNR (from -0.26 ± 0.06 m w.e. a^{-1} in1976-2000 to -0.37±0.15 m w.e. a^{-1} in 2000-2020), is similar to the broader regional pattern of accelerating loss across the Himalayas and Kangri Karpo Mountains (Maurer et al., 2019; Wu et al., 2018, 2019).

4.2 The influences of debris-cover and proglacial lakes on glacier mass changes

Debris can inhibit or enhance glacial ablation depending on its thickness (Maurer et al., 2016). A shallow layer of debris usually enhance melt rates due to its low surface albedo, while thicker layers could suppress melt rates through thermal insulation (Reid et al., 2012). Our results (Table 3) suggest that the debris-covered glaciers in our study thinned more slowly

than the regular, debris-free glaciers in the 1976-2000 period, though the difference is not statistically significant and the small sample size (5) of the debris-covered glaciers compared to regular glaciers (>600) limits our ability to compare these classes. In the 2000-2020 period, the thinning rate of the debris-covered glaciers increased significantly, to double its previous rate, though it remains indistinguishable from the thinning rate for regular glaciers at that time. While several previous studies indicated that on the glacier-scale, debris-covered glaciers thin more slowly than debris-free glaciers(Nicholson & Benn, 2006; Scherler et al., 2011; Vincent et al., 2016), large-scale geodetic studies reported no significant differences in the thinning rates between debris-covered and clean glaciers on time scales more than a decade after 2000 (Brun et al., 2019; Ke et al., 2020; Maurer et al., 2019), a finding that is supported by this study. Banerjee (2017) suggested that the thinning rate of a debris-covered glacier is initially slower than that of a similar clean glacier at the early stage of warming but subsequently matches and then overtakes the clean counterpart. In this theory, the time required for their respective melting rates to cross is controlled by the rate of warming, with little difference between their thinning rates at low rates of warming (Banerjee, 2017). The large difference in the 1976-2000 mean melt rates of the regular versus debris-covered glaciers in our study provides some supports for this theory, but a larger sample with lower uncertainty is needed to verify this.

For debris-covered glaciers, the area of debris cover actually increased from 6.60 ± 1.15 km^2 in 1976 to 7.37 ± 1.48 km^2 in 2020 in our study (Table S6), and we note that this is not necessarily inconsistent with an overall glacier retreat. This is because increased melt rates that lead to surface lowering drive retreat of the glacier front, while also promoting a greater concentration of debris on the wider surface of glacier ablation area as more debris melts out from ice below. A spatial expansion of the debris layer has, for example, been observed on different debris-covered glaciers during retreat and sustained mass loss. (Kirkbride & Deline, 2013; Stokes et al., 2007; Tielidze et al., 2020; Xie et al., 2020). Unfortunately, no data are available relating to changes of the thickness of the debris cover itself, and we assume that all glacier thickness changes resulted from loss of ice, without considering the thickness change of the debris cover layer. We think that this is reasonable in because in most area, debris layers are typically thin (order of 1 meter or less) and compared to elevation changes we map, and because most debris cover in the ablatio area emerge from englacial transport rather than direct deposition by new, local rock fall(e.g., McCarthy et al. 2017), so changes in the debris-layer thickness represent a redistribution of existing glacier volume, not a change in volume.

Glaciers with proglacial lakes can experience relatively high mass loss through calving and thermal undercutting (Maurer et al., 2016; Thompson et al., 2012) and the expansion of such lakes can cause dynamic thinning to propagate up-glacier (Ke et al., 2020). Glaciers terminating in proglacial lakes in our study area had the highest mean thinning rates of all the classes in both time periods, and more negative mass balance compared to both regular and debris covered glacier during 2000-2020.

The area of debris-covered glaciers and lake-terminating glaciers decreased, while surface lowering also accelerated, mainly driven by the continuous increase in temperature in the WNR region during 1976-2000, especially after 2014 (Figure 12 and Figure 13), which was discussed in 4.3. In terms of the number and area of lake-termination, we identified glacier-

364   marginal lakes as those lying within 50 m of a glacier boundary. As glaciers retreat, the distance between the end of the glacier

365   and their proglacial lake increased, and some of lake-terminating glaciers in 1976 no longer belonged to lake-terminating class

366   in 2000. This helps for explain the area decreased for this glacier class in Table 3.

4.3 Topographic and climatic controls of varying glacier mass loss

368   If climate is the driving force behind glacier change, topographical parameters can modulate this change (Pandey et al.,

369   2017). Controls on glacier thickness and areal change are complicated, however, with additional factors including local

370   variations in climate, glacier thickness, morphology, the presence of proglacial/supraglacial lakes and debris cover, and latitude

371   and longitude (Brun et al., 2018b,2019; Ke et al.,2020; Maurer et al., 2019).

372   We found that both glacier areal retreat rate (Figure 4b) and thinning rate (Figures 8 and 9) generally decreased with

373   increasing altitude, agreeing with previous studies (Li & Lin, 2017; Wu et al., 2016; Ye et al., 2017; Zhou et al., 2019). However,

374   the effect of slope and aspect on glacier thickness has been rarely studied. We found that in the slope range of 8-40°, where

375   the glaciers were mainly distributed, the rate of areal retreat increased as slope increased (Figure 4c), but the thinning rate

376   decreased (Figure 8b). This occurred because steep slopes are associated with thinner ice (Linsbauer et al., 2012), which

377   means that any given thinning rate will tend to drive more rapid areal retreat on steeper slopes as the thinner ice there is

378   depleted first, explaining the broadly positive correlation between retreat and slope. Besides, steeper slopes are biased

379   towards higher elevations, where the colder climate leads to slower thinning rates (dh), explaining the broadly negative

380   correlation between slope and thinning rate. The somewhat different behavior of the low-elevation flat areas (relatively

381   rapid retreat, relatively slow thinning, Figure 9) may in part reflect the modulating effects of proglacial lakes (quicker

382   retreat) and thicker debris cover (slower thinning) near the terminus. Overall, the relationship between aspect and both

383   areal retreat and thinning was spatially inconsistent and varied in time (Figures 4d and 8c).

384   Mean glacier mass thinning and retreat rates were consistently higher in the Nam Co basin than Lhasa River basin (Table

385   1 and 2), in agreement with Bolch et al.(2010) and Li & Lin (2017), and the glaciers in central WNR showed particularly

386   strong melting from 2000 to 2020. While the glacier distribution on the TP broadly follows the regional atmospheric circulation

387   pattern (Yao et al., 2012), the variability in glacier loss within regions cannot always be fully explained by the changes in

388   precipitation and temperature on this scale (Wu et al., 2018).

389   The increasingly-negative mass balance through time is consistent with the temperature record from the three weather

390   stations that shows a consistent warming trend (averaging 0.0485 °C a^{-1}) (Figure 12) and gridded temperature data showing a

391   more rapid increase during 2000-2018 than 1979-2000 (Figure 13), alongside precipitation that increased during 1979-2020

392   but decreased during 2000-2018. The accelerated warming from 2014 to 2018 (red rectangle in Figure 13 (2014-2018))

393   corresponds geographically to the substantial central-WNR glacier thinning highlighted in the red rectangle in Figure 5.

394   Precipitation also increased substantially in this region from 2014 to 2018, and glacier melting can be particularly intense

395   under combined warm and wet conditions (Li et al., 2020; Oerlemans & Fortuin, 1992).

396   While the overall, the trends of temperature and precipitation in the ablation season (June to September) and

397   accumulation season (October to December and January to May) were similar to annual changes, the temperature and

398   precipitation data from 2014 to 2018 described above offer a compelling explanation for the main temporal and spatial

399   variations in glacier change in the WNR, particularly the high rates of thinning from 2014-2018. They do not directly explain

400   why the Nam Co glaciers thinned more rapidly than elsewhere, however. Other possible explanations include difference in the

401   impact of black carbon and dust in reducing surface albedo (Lau et al., 2010; Li & Lin, 2017; Ming et al., 2008), and Qu et al.

402   (2014) did observe a decrease in albedo at Zhadang glacier (Nam Co basin) from 2001-2012.

403   **4.4 Hydrological effect**

404   The glacier melt contribution to streamflow decreases significantly from the glacier terminus to the lowlands as it

405   becomes diluted by other water sources (Kaser et al.,2010; Lutz et al., 2014; Pritchard, 2019) and this is reflected in our

406   finding that the average annual glacier mass loss during 1976-2014 (-0.26 ± 0.14 m w.e.a^{-1}) equates to $8.5\pm4.6\%$ of the mean

407   annual runoff depth for the Yangbajain basin, in the upper reaches of Lhasa River (location shown in Figure 1(a)), but only

408    $1.6\pm1.0\%$ for the Lhasa Riber basin as a whole.

409   Through this period, the annual runoff in the Yangbajain basin showed a significant increase trend of 1.32 mm a^{-1} and

410   the Lhasa River basin a non-significant increase trend of 0.84 mm a^{-1} (Figure S4). Increasing runoff may in part be explained

411   by a coincident 1.36 mm a^{-1} increase in precipitation observed over the Lhasa River basin (Figure 12(b)), though the glacier

412   ablation increase in Lhasa River basin and Yangbajain basin (4.63 ± 2.49 mm a^{-1} and 23.52 ± 12.67 mm a^{-1} respectively) were

413   substantially greater than the increase in precipitation, and evaporation losses from glacier melt water tend to be substantially

414   smaller than those from evaporation of precipitation over the basin (Pritchard, 2019), suggesting that increased glacial

415   meltwater primarily drove increased runoff. This is supported by Lin et al. (2020) who attributed increase streamflow at

416   Yangbajain Station to accelerated glacier retreat, and Wang et al. (2021b) who argued that glacier melt has increased its

417   contributions to the surface runoff by 12%-43% among the sub-basins of the Yarlung-Zangpo River basin (the mainstream

418   of Lhasa River) after 1997.

419   Some components of basin hydrology remain poorly observed, however we note that the combined increase in

420   precipitation and ablation detailed above was much notably greater than the observed increase in runoff especially in the

421   Yangbajain, a discrepancy that due to some combination of increased residential, industrial or agricultural water use

422   (Pritchard, 2019), increased evaporation (Han et al., 2021), and possible deep seeps in upper Lhasa River (Lin et al., 2020).

423   In the Nam Co basin, increase glacier runoff also appears to have been important in controlling the level of Nam Co

424   Lake. The Nam Co basin glacier mass balance (0.32 ± 0.16 m w.e.a^{-1}) that we found for 1976-2014, equated to $30.9 \pm 15.4\%$

425   of the reported increase in Nam Co Lake water storage (Zhang et al., 2011b). This glacier contribution is comparable to

426 previous estimates of 52.9% for the 1971-2004 period (Zhu et al., 2009), 28.7% for 1999-2010 based on a mass balance of

427 0.59 m w.e.a^{-1} (Zhadang glacier) (Lei et al., 2013), 10.50 ± 9.00% for 2003-2009 by based on a mass balance of -0.27±0.13

428 m w.e. a^{-1} (Li & Lin (2017), and 17.5±7.6% for 2000-2014 based on a mass balance of -0.32 m w.e. a^{-1} (Ke et al., 2022).

429 Differences in these contributions of glaciers to increases in lake level reflect differences in the time periods studied and

430 variability in the rate of change in the lake. For example, Ke et al. (2022) reported that their average lake level change of

431 (0.26 ± 0.04 m a^{-1} for 2000s–2014) is substantially higher than 0.14± 0.18 m a^{-1} for 1994–2015 reported by Brun et al.

432 (2020).

5. Conclusions

434 Based on KH-9, Landsat, SRTM and ASTER satellite data, we have quantified the changes of glacier area, surface

435 elevation and mass balance in the WNR over the past 44 years and compared the effects of topography, debris-cover and

436 proglacial lakes on glacier change during 1976-2000 and 2000-2020. Our major conclusions are:

437 (1) Glaciers in the WNR retreated by 295.73 ± 43.45km^2, or 33.42 ± 4.9% of their area, from 1976-2020, at a mean rate

438 of -0.76 ± 0.11 % a^{-1}. Over this time, they lost a total of 11.56 ±0.12 Gt of ice. In addition, increased glacial meltwater in the

439 WNR primarily drove increased runoff in Lhasa River basin and appeared to have been important in controlling the level of

440 Nam Co Lake. The Nam Co basin glacier mass balance (0.32±0.16 m w.e.a^{-1} during 1976-2014), equated to 30.9 ± 15.4% of

441 the increase in Nam Co Lake water storage.

442 (2) The average retreat rate from 2000 to 2020 (1.17 ± 0.30 % a^{-1}) was more than twice that from 1976 to 2000 (0.54 ±

443 0.21 % a^{-1}). Similarly, the mean glacier mass balance from 2000 to 2020 (-0.37 ± 0.12 m w.e.a^{-1}) was more negative than that

444 from 1976 to 2000 (-0.26 ± 0.09 m w.e.a^{-1}) (though the change is within the uncertainties). The more rapid ice loss from 2000

445 to 2020 was mainly due to intensified glacier melting after 2014, which was likely associated with particularly strong warming

446 of the region after that year. Besides, areal retreat rate and mass loss rate of most glaciers was not synchronized during 1976-

447 2000 and 2000-2020.

448 (3) In the WNR the spatial and temporal patterns of glacier loss can largely be explained by the observed patterns of

449 regional climate change. Locally, the mass balance varied between different types of glaciers with proglacial lakes associated

450 with the most rapid loss, particularly during 2000-2020. The mass balance of debris-covered glaciers was similar to debris-

451 free glaciers during 2000-2020.

452 (4) Topographic setting influenced retreat and thinning, with loss rates decreasing with increasing elevation. The rate of

453 both glacier retreat and thinning decreased with elevation, but the relationship between the parameters of slope and aspect with

454 thinning rates differed from their relationship with retreat rates, spatially and through time. For slopes of 8-40° (which includes

455 most glaciers), for example, the retreat rate increased with slope while the thinning rate decreased.

456 In this study, we observed accelerated glacier loss in the WNR on multi-year time scales. However, factors such as

precipitation, temperature and altitude could not yet fully explain the heterogeneity of glacier changes. Thus, more detail data and glacier ablation models are needed to fully understand the mechanism of glacier change in the future.

Code and data availability. All codes and data in this paper are available upon request to the corresponding author. The sources of data used in this paper are listed in section 2.2 and are accessible via their websites.

Competing interests. The authors declare that they have no conflict of interests.

Author contributions. Conceptualization, S.W.; methodology, S.W.; software, S.W. and X.Q.; data curation, S.W., and J.Z; writing—original draft preparation, S.W.; writing—review and editing, H.P. and L.K.; visualization, H.P and J.L.; supervision, W.X. and Y.Z.; project administration, J.L.; funding acquisition, J.L.

Acknowledgements. We would like to thank editor Fuqiang Tian, Xiangying Li and the two anonymous reviewers for their valuable comments that have made improvements in the contents of this paper.

Financial support. This work was supported by the Second Tibetan Plateau Scientific Expedition and Research Program (STEP; Ministry of Science and Technology, MOST; grant no. 2019QZKK0207), the National Natural Science Foundation of China (NSFC; grant no. 92047301).

References:

Bahr, D. B., Meier, M. F., & Peckham, S. D.: The physical basis of glacier volume-area scaling, J Geophys Res-Sol Ea, 102(B9), 20355–20362, https://doi.org/10.1029/97JB01696, 1997.

Bahr, D. B., Pfeffer, W. T., & Kaser, G.: A review of volume-area scaling of glaciers, Rev Geophys, 53(1), 95–140. https://doi.org/10.1002/2014RG000470, 2015.

Banerjee, A.: Brief communication: thinning of debris-covered and debris-free glaciers in a warming climate, Cryosphere, 11(1), 133-138. https://doi.org/10.5194/tc-11-133-2017, 2017.

Bolch, T., Yao, T., Kang, S., Buchroithner, M. F., Scherer, D., & Schneider, C., et al.: A glacier inventory for the western Nyainqentanglha range and the Nam Co Basin, Tibet, and glacier changes 1976-2009, Cryosphere, 4(3), 419-433, https://doi.org/10.5194/tc-4-419-2010, 2010.

Brun, F., Berthier, E., Wagnon, P., Kääb, A., & Treichler, D.: A spatially resolved estimate of High Mountain Asia glacier mass balances, 2000-2016. Nat Geosci, 10(9), 668–673, https://doi.org/10.1038/s41561-018-0171-z, 2018a.

Brun, F., Treichler, D., Shean, D., Immerzeel, W.W.: Limited contribution of glacier mass loss to the recent increase in Tibetan plateau Lake volume, Front. Earth Sci. 8, 582060, https://doi.org/10.3389/feart.2020.582060, 2020.

Brun, F., Wagnon, P., Berthier, E., Jomelli, V., Maharjan, S. B., & Kraaijenbrink, P. D. A., et al.: Heterogeneous Influence of Glacier Morphology on the Mass Balance Variability in High Mountain Asia, J Geophys Res-Sol Ea, 124(6), 1331–1345,

https://doi.org/10.1029/2018JF004838, 2019.

Brun, F., Wagnon, P., Berthier, E., Shea, J. M., & Immerzeel, W. W.: Ice cliff contribution to the tongue-wide ablation of Changri Nup Glacier, Nepal, central Himalaya, Cryosphere, 12(11), 3439-3457, https://doi.org/10.5194/tc-12-3439-2018, 2018b.

Ding, L., Zhou, J., Wang, W.: Dataset of 0.01° Surface Air Temperature over Tibetan Plateau (1979-2018), National Tibetan Plateau Data Center, 10.11888/Meteoro.tpdc.270339. CSTR: 18406.11.Meteoro.tpdc.270339, 2020.

Duan, A., & Xiao, Z.: Does the climate warming hiatus exist over the Tibetan Plateau? Sci Rep-UK. 5, 13711, https://doi.org/10.1038/srep13711, 2015.

Frauenfelder, R., & Kääb, A.: Glacier mapping from multi-temporal optical remote sensing data within the Brahmaputra River Basin, In Proceedings of the 33rd International Symposium on Remote Sensing of Environment, 4-8, 2009.

Gardelle, J., Berthier, E., Arnaud, Y., Kääb, A.: Region-wide glacier mass balances over the Pamir-Karakoram-Himalaya during 1999–2011, Cryosphere 7, 1263–1286, https://doi.org/10.5194/tc-7-1263-2013, 2013.

Guo, W., Liu, S., Xu, J., Wu, L., Shangguan, D., & Yao, X., et al.: The second chinese glacier inventory: data, methods and results, J Glaciol. 61(226), 357-372, https://doi.org/10.3189/2015JoG14J209, 2015.

Han, C., Ma, Y., Wang, B., Zhong, L., Ma, W., Chen, X., & Su, Z.: Long-term variations in actual evapotranspiration over the Tibetan Plateau, Earth Syst. Sci. Data, 13(7), 3513-3524, https://doi.org/10.5194/essd-13-3513-2021, 2021.

He, J., Yang, K., Tang, W., Lu, H., Qin, J., & Chen, Y., et al.: The first high-resolution meteorological forcing dataset for land process studies over China, Sci Data, 7,25, https://doi.org/10.1038/s41597-020-0369-y, 2020.

Kääb, A., Berthier, E., Nuth, C., Gardelle, J., & Arnaud, Y.: Contrasting patterns of early twenty-first-century glacier mass change in the Himalayas, Nature, 488(7412), 495-498, https://doi.org/10.1038/nature11324, 2012.

Kaser, G., Großhauser, M., & Marzeion, B.: Contribution potential of glaciers to water availability in different climate regimes, Proc. Natl Acad. Sci, USA 107, 20223–20227, https://doi.org/10.1073/pnas.1008162107, 2010.

Ke, L., Song, C., Wang, J., Sheng, Y., Ding, X., Yong, B., et al.: Constraining the contribution of glacier mass balance to the Tibetan lake growth in the early 21st century, Remote Sens Environ, 268, 112779, DOI: 10.1016/j.rse.2021.112779, 2022.

Ke, L., Song, C., Yong, B., Lei, Y., & Ding, X.: Which heterogeneous glacier melting patterns can be robustly observed from space? A multi-scale assessment in southeastern Tibetan Plateau, Remote Sens Environ, 242, https://doi.org/10.1016/j.rse.2020.111777, 2020.

Kirkbride, M. P., & Deline, P.: The formation of supraglacial debris covers by primary dispersal from transverse englacial ebris bands, Earth Surf Process Landf, 38(15), 1779-1792, https://doi.org/10.1002/esp.3416, 2013.

Lau, W., Kim, M. K., Kim, K. M., & Lee, W. S.: Enhanced surface warming and accelerated snow melt in the Himalayas and Tibetan Plateau induced by absorbing aerosols, Environ. Res. Lett, 5(2), 025204, https://doi.org/10.1088/1748-

518   9326/5/2/025204, 2010.

519   Lei, Y., Yao, T., Bird, B. W., Yang, K., Zhai, J., & Sheng, Y.: Coherent Lake growth on the central Tibetan Plateau since

520   the 1970s: Characterization and attribution, J Hydrol, 483, 61-67, http://dx.doi.org/10.1016/j.jhydrol.2013.01.003,

521   2013.

522   Li, Y. J., Ding, Y.J., Shangguan, D. H., & Wang, R. J.: Regional differences in global glacier retreat from 1980 to 2015 -

523   sciencedirect, Adv. Clim. Chang. Res., 10(4), 203-213. https://doi.org/10.1016/j.accre.2020.03.003, 2020.

524   Li, G., & Lin, H.: Recent decadal glacier mass balances over the Western Nyainqentanglha Mountains and the increase in their

525   melting contribution to Nam Co Lake measured by differential bistatic SAR interferometry, Global Planet Change, 149,

526   177-190, https://doi.org/10.1016/j.gloplacha.2016.12.018, 2017.

527   Lin, L., Gao, M., Liu, J., Wang, J., Wang, S., & Chen, X., et al.: Understanding the effects of climate warming on streamflow

528   and active groundwater storage in an alpine catchment: The upper Lhasa River, Hydrol Earth Syst Sc. 24(3), 1145-1157,

529   https://doi.org/10.5194/hess-24-1145-2020, 2020.

530   Linsbauer, A., Paul, F., & Haeberli, W.: Modeling glacier thickness distribution and bed topography over entire mountain

531   ranges with GlabTop: Application of a fast and robust approach, Journal of Geophysical Research: Earth Surface, 117(F3),

532   https://doi.org/10.1029/2011JF002313, 2012.

533   Luo, W., Zhang, G., Chen, W., & Xu, F.: Response of glacial lakes to glacier and climate changes in the western

534   Nyainqentanglha range, Sci Total Environ. 735, 139607, https://doi.org/10.1016/j.scitotenv.2020.139607, 2020.

535   Lutz, A. F., Immerzeel, W. W., Shrestha, A. B., & Bierkens, M. F. P.: Consistent increase in High Asia's runoff due to increasing

536   glacier melt and precipitation, Nat Clim Change, 4(7), 587–592, https://doi.org/10.1038/nclimate2237, 2014.

537   Maurer, J. M., Schaefer, J. M., Rupper, S., & Corley, A.: Acceleration of ice loss across the Himalayas over the past 40 years,

538   Sci Adv. 5(6), aav7266, https://doi.org/10.1126/sciadv.aav7266, 2019.

539   Maurer, J., & Rupper, S.: Tapping into the Hexagon spy imagery database: A new automated pipeline for geomorphic change

540   detection, ISPRS J Photogramm. 108, 113-127, https://doi.org/10.1016/j.isprsjprs.2015.06.008, 2015.

541   Maurer, J. M., Rupper, S. B., & Schaefer, J. M.: Quantifying ice loss in the eastern himalayas since 1974 using declassified

542   spy satellite imagery, Cryosphere, 10(5), 2203-2215, https://doi.org/10.5194/tc-10-2203-2016, 2016.

543   McCarthy, M., Pritchard, H., Willis, I. A. N., & King, E.: Ground-penetrating radar measurements of debris thickness on

544   Lirung Glacier, Nepal, J Glaciol, 63(239), 543-555, https://doi.org/10.1017/jog.2017.18, 2017.

545   Ming, J., Cachier, H., Xiao, C., Qin, D., Kang, S., & Hou, S., et al.: Black carbon record based on a shallow Himalayan ice

546   core and its climatic implications,   Atmos Chem Phys, 8(5), 1343–1352, https://doi.org/10.5194/acp-8-1343-2008, 2008.

547   Neckel, N., Kropá,J., Bolch, T., & Hochschild, V.: Glacier mass changes on the Tibetan Plateau 2003 – 2009 derived from

548   ICESat laser altimetry measurements, Environ Res Lett, 9(1), 468-475, https://doi.org/10.1088/1748-9326/9/1/014009, 2014.

549   Nicholson, L., & Benn, D.: Calculating ice melt beneath a debris layer using meteorological data, J Glaciol, 52(178),

463-470, https://doi.org/10.3189/172756506781828584, 2006.

Nie, Y., Pritchard, H. D., Liu, Q., Hennig, T., Wang, W., Wang, X., et al.: Glacial change and hydrological implications in the Himalaya and Karakoram, Nat. Rev. Earth Environ, 2(2), 91-106, https://doi.org/10.1038/ s43017-020-00124- w, 2021.

Nuth, C., & Kääb, A.: Co-registration and bias corrections of satellite elevation data sets for quantifying glacier thickness change, Cryosphere, 5(1), 271-290, https://doi.org/10.5194/tc-5-271-2011, 2011.

Oerlemans, J., & Fortuin, J.: Sensitivity of Glaciers and Small Ice Caps to Greenhouse Warming. Science, 258(5079), 115-117, https://doi.org/10.1126/science.258.5079.115, 1992.

Pandey, P., Ali, S. N., Ramanathan, A. L., Champati ray, P. K., & Venkataraman, G.: Regional representation of glaciers in Chandra Basin region, western Himalaya, India, Geosci Front. 8(4), 841–850, https://doi.org/10.1016/j.gsf.2016.06.006, 2017.

Pritchard, H. D.: Asia's shrinking glaciers protect large populations from drought stress. Nature.569(7758), 649-654, https://doi.org/10.1038/s41586-019-1240-1, 2019.

Qiao, X., Liu, J., Wang, S., Wang, J., Ji, H., Chen, X., et al.: Lead-lag correlations between snow cover and meteorological factors at multi-time scales in the Tibetan Plateau under climate warming, Theor. Appl. Climatol, 146(3), 1459-1477, https://doi.org/10.1007/s00704-021-03802-x, 2021.

Qu, B., Ming, J., Kang, S. C., Zhang, G. S., Li, Y. W., & Li, C. D. et al.: The decreasing albedo of the Zhadang glacier on western Nyainqentanglha and the role of light-absorbing impurities, Atmos Chem Phys.14(20), 11117-11128, https://doi.org/10.5194/acp-14-11117-2014, 2014.

Reid, T. D., Carenzo, M., Pellicciotti, F., & Brock, B. W.: Including debris cover effects in a distributed model of glacier ablation, J Geophys Res-Atmos, 117(D18), https://doi.org/10.1029/2012JD017795, 2012.

Ren, S., Menenti, M., Jia, L., Zhang, J., & Li, X.: Glacier Mass Balance in the Nyainqentanglha Mountains between 2000 and 2017 Retrieved from ZiYuan-3 Stereo Images and the SRTM DEM, Remote Sens, 12(5), 864-, https://doi.org/10.3390/rs12050864, 2020.

RGI Consortium.: Randolph Glacier Inventory – A Dataset of Global Glacier Outlines: Version 6.0, July, 1–27, https://ci.nii.ac.jp/naid/40021243259/, 2017.

Scherler, D., Bookhagen, B., & Strecker, M. R.: Spatially variable response of himalayan glaciers to climate change affected by debris cover, Nat Geosci, 4(3), 156-159, https://doi.org/10.1038/ngeo1068, 2011.

Shangguan, D. H., Liu, S. Y., Ding, L. F., Zhang, S. Q., Gang, L. I., & Zhang, Y., et al.: Variationof Glaciers inthe Western Nyainqêntanglha Range ofTibetanPlateauduring1970 − 2000, Journal of Glaciology and Geocryology, 2008. (In Chinese)

Stokes, C. R., Popovnin, V., Aleynikov, A., Gurney, S. D., & Shahgedanova, M.: Recent glacier retreat in the Caucasus Mountains, Russia, and associated increase in supraglacial debris cover and supra-/proglacial lake development, Ann. Glaciol, 46, 195-203, https://doi.org/10.3189/172756407782871468, 2007.

Su,F., Zhang, L., Ou, T., Chen, D., Yao, T., & Tong, K., et al.: Hydrological response to future climate changes for the major upstream river basins in the Tibetan Plateau, Global Planet Change, 136, 82-95, https://doi.org/10.1016/j.gloplacha.2015.10.012, 2016.

Surazakov, A., & Aizen, V.: Positional accuracy evaluation of declassified hexagon KH-9 mapping camera imagery, Photogramm Eng Rem S, 76(5), 603-608, https://doi.org/10.14358/PERS.76.5.603, 2010.

Tielidze, L. G., Bolch, T., Wheate, R. D., Kutuzov, S. S., Lavrentiev, I. I., & Zemp, M.: Supra-glacial debris cover changes in the Greater Caucasus from 1986 to 2014, Cryosphere, 14(2), 585-598, https://doi.org/10.5194/tc-14-585-2020, 2020.

Thompson, S. S., Benn, D. I., Dennis, K., & Luckman, A.: A rapidly growing moraine-dammed glacial lake on Ngozumpa Glacier, Nepal. Geomorphology, 145–146, 1–11, https://doi.org/10.1016/j.geomorph.2011.08.015, 2012.

Vincent, C., Wagnon, P., Shea, J. M., Immerzeel, W. W., Kraaijenbrink, P., & Shrestha, D., et al.: Reduced melt on debris-covered glaciers: Investigations from Changri Nup Glacier, Nepal, Cryosphere, 10(4), 1845-1858, https://doi.org/10.5194/tc-10-1845-2016, 2016.

Viviroli, D., Dürr, H. H., Messerli, B., Meybeck, M., & Weingartner, R.: Mountains of the world, - water towers for humanity: Typology, mapping, and global significance, Water Resour Res. 43(7), https://doi.org/10.1029/2006WR005653, 2007.

Wang, J. R., Chen, X., Liu, J. T., & Qi, H.: Changes of Precipitation–Runoff Relationship Induced by Climate Variation in a Large Glaciated Basin of the Tibetan Plateau, J. Geophys. Res.-Atmos, 126(21), https://doi.org/10.1029/2020JD034367, 2021b.

Wang, Q., Yi, S., & Sun, W.: Continuous Estimates of Glacier Mass Balance in High Mountain Asia Based on ICESat-1,2 and GRACE/GRACE Follow-On Data, Geophys Res Lett, 48(2). https://doi.org/10.1029/2020GL090954, 2021a.

Wang, X., Zhou, A. G., Siegert, F., Zhang, Z., & Chen, K. L.: Glacier temporal-spatial change characteristics in western Nyainqentanglha Range, Tibetan Plateau 1977-2010, Earth Science - Journal of China University of Geosciences, 37(5): 1082-1092, 2012. (In Chinese)

Wu, G., Duan, A., Liu, Y., Mao, J., Ren, R., & Bao, Q., et al.: Tibetan Plateau climate dynamics: Recent research progress and outlook, Natl Sci Rev, 2(1), 100–116, https://doi.org/10.1093/nsr/nwu045, 2015.

Wu, K. P., Liu, S., Jiang, Z., Xu, J. L., & Wei, J.: Glacier mass balance over the central Nyainqentanglha Range during recent decades derived from remote-sensing data, J Glaciol.65(251), 422–439, https://doi.org/10.1017/jog.2019.20, 2019.

Wu, K. P., Liu, S., Jiang, Z., Xu, J., Wei, J., & Guo, W.: Recent glacier mass balance and area changes in the kangri karpo mountains from dems and glacier inventories, The Cryosphere. 12(1), 103-121, https://doi.org/10.5194/tc-12-103-2018, 2018.

Wu, K. Q., Liu, S. Y., Guo, W. Q., Wei, J. F., Xu, J. L., & Bao, W. J., et al.: Glacier change in the western Nyainqentanglha Range, Tibetan Plateau using historical maps and Landsat imagery: 1970-2014, J MT Sci Engl, 13(8), 1358–1374,

614   https://doi.org/10.1007/s11629-016-3997-0, 2016.

615   Wu, Y., & Zhu, L.: The response of lake-glacier variations to climate change in Nam Co Catchment, central Tibetan Plateau,

616   during 1970–2000, J Geogr Sci, 18(2), 177-189, https://doi.org/10.1007/s11442-008-0177-3, 2008.

617   Yang, K., He, J., Tang, W., Qin, J., & Cheng, C.: On downward shortwave and longwave radiations over high altitude regions:

618   Observation   and   modeling   in   the   Tibetan   Plateau,   Agr   Forest   Meteorol,150(1),   38-46,

619   https://doi.org/10.1016/j.agrformet.2009.08.004, 2010.

620   Yao, T. D., Li, Z. G., Yang, W., Guo, X. J., Zhu, L. P., & Kang, S. C., et al.: Glacial distribution and mass balance in the Yarlung

621   Zangbo river and its influence on lakes, Chinese Sci Bull, 55(20), 2072–2078, https://doi.org/10.1007/s11434-010-3213-5,

622   2010.

623   Yao, T. D., Pu, J., Lu, A., Wang, Y., & Yu, W.: Recent glacial retreat and its impact on hydrological processes on the tibetan

624   Plateau, China, and surrounding regions, Arct Antarct Alp Res., 39(4), 642-650, https://doi.org/10.1657/1523-0430(07-

625   510)[YAO]2.0.CO;2, 2007.

626   Yao, T. D., Thompson, L., Yang, W., Yu, W., Gao, Y., & Joswiak, D.: Different glacier status with atmospheric circulations in

627   tibetan plateau and surroundings, Nat Clim Change, 2(9), 663–667, https://doi.org/10.1038/NCLIMATE1580, 2012.

628   Ye, Q., Zong, J., Tian, L., Cogley, J. G., Song, C., & Guo, W.: Glacier changes on the Tibetan Plateau derived from Landsat

629   imagery: Mid-1970s - 2000-13, J Glaciol, 63(238), 273–287, https://doi.org/10.1017/jog.2016.137, 2017.

630   Yu, W., Yao, T., Kang, S., Pu, J., Yang, W., & Gao, T., et al.: Different region climate regimes and topography affect the changes

631   in area and mass balance of glaciers on the north and south slopes of the same glacierized massif (the West Nyainqentanglha

632   Range, Tibetan Plateau), J Hydrol, 495, 64-73, https://doi.org/10.1016/j.jhydrol.2013.04.034, 2013.

633   Xie, Z., Haritashya, U. K., Asari, V. K., Young, B. W., Bishop, M. P., & Kargel, J. S.: GlacierNet: A deep-learning

634   approach   for   debris-covered   glacier   mapping,   IEEE   Access,   8,   83495-83510,   https://doi.org/

635   10.1109/ACCESS.2020.2991187, 2020.

636   Zhang, G., Yao, T., Shum, C. K., Yi, S., Yang, K., & Yu, J., et al.: Lake volume and groundwater storage variations in tibetan

637   plateau's   endorheic   basin,   Geophys   Res   Lett,   44(11),   5550-5560,   44(11),   5550–5560,

638   https://doi.org/10.1002/2017GL073773, 2017.

639   Zhang, Q., & Zhang, G.: Glacier elevation changes in the western nyainqentanglha range of the Tibetan Plateau as observed

640   by TerraSAR-X/TanDEM-X images, Remote Sens Lett, 8(12), 1143-1152. https://doi.org/10.1080/2150704X.2017.1362123,

641   2017.

642   Zhang, S.Q., Gao, X., Ye, B.S., Zhang, X.W., Stefan, H.: A modified monthly degree-day model for evaluating glacier runoff

643   changes in China part II: application, Hydrol Process, 26(11), 1697-1706, https://doi.org/10.1002/hyp.8291, 2011a.

644   Zhang, B., Wu, Y., Zhu, L., Wang, J., Li, J., & Chen, D.: Estimation and trend detection of water storage at Nam Co

645   Lake, central Tibetan Plateau, J Hydrol, 405(1-2), 161-170, https://doi.org/10.1016/j.jhydrol.2011.05.018, 2011b.

646 Zhao, Q., Ding, Y., Wang, J., Gao, H., Zhang, S., & Zhao, C., et al.: Projecting climate change impacts on hydrological

647 processes on the Tibetan Plateau with model calibration against the glacier inventory data and observed streamflow, J Hydrol,

648 573, 60-81, https://doi.org/10.1016/j.jhydrol.2019.03.043, 2019.

649 Zhou, S., Kang, S., Feng, C., & Joswiak, D. R.: Water balance observations reveal significant subsurface water seepage from

650 Lake Nam Co, south-central Tibetan Plateau, J Hydrol, 491(1), 89-99, https://doi.org/10.1016/j.jhydrol.2013.03.030, 2013.

651 Zhou, Y., Hu, J., Li, Z., Li, J., Zhao, R., & Ding, X.: Quantifying glacier mass change and its contribution to lake growths in

652 central Kunlun during 2000–2015 from multi-source remote sensing data, J Hydrol, 570, 38–50,

653 https://doi.org/10.1016/j.jhydrol.2019.01.007, 2019.

654 Zhou, Y., Li, Z., Li, J., Zhao, R., & Ding, X. Glacier mass balance in the Qinghai–Tibet Plateau and its surroundings from the

655 mid-1970s to 2000 based on Hexagon KH-9 and SRTM DEMs, Remote Sens Environ, 210, 96-112,

656 https://doi.org/10.1016/j.rse.2018.03.020, 2018.

657 Zhu, L., Xie, M., & Wu, Y.: Quantitative analysis of lake area variations and the influence factors from 1971 to 2004 in

658 the Nam Co basin of the Tibetan Plateau, Chinese Sci Bull, 55(13), 1294-1303, https://doi.org/10.1007/s11434-010-

659 0015-8, 2010.

660 Table 1 Glacier area changes over the WNR from 1976 to 2020

	1976 Area(km^2)	2000 Area (km^2)	2020 Area (km^2)	1976-2000 △Area (% a^{-1})	2000-2020 △Area (% a^{-1})	1976-2020 △Area (% a^{-1})
The WNR	884.90±29.71	770.03±33.44	589.17±31.72	-0.54± 0.21	-1.17± 0.30	-0.76± 0.11
Lhasa River	662.23±21.95	580.81±22.79	447.93±21.74	-0.51± 0.20	-1.14± 0.27	-0.74± 11
Nam Co basin	222.58±7.76	189.22±7.62	141.22±7.10	-0.62± 0.20	-1.27± 0.32	-0.83± 0.11

661 Table 2 Glacier elevation change, mass balance and total mass change over the WNR from 1976 to 2020

	1976-2000			2000-2020		
	Elevation change (m a^{-1})	Mass Balance (m w.e.a^{-1})	Total mass change (Gt a^{-1})	Elevation change (m a^{-1})	Mass Balance (m w.e.a^{-1})	Total mass change (Gt a^{-1})
The WNR	-0.31 ± 0.10	−0.26± 0.09	−0.24± 0.08	−0.44± 0.13	−0.37± 0.12	−0.29± 0.09
Lhasa River	-0.29± 0.12	−0.25± 0.10	−0.21± 0.10	−0.40± 0.16	−0.34± 0.14	−0.26± 0.09
Nam Co basin	-0.36 ± 0.17	−0.31 ± 0.15	−0.06± 0.02	−0.52± 0.18	−0.44± 0.16	−0.06 ± 0.03

662 Table 3 Statistics of area, quantity, and mass balance of different types of glaciers

Glacier type	1976-2000			2000-2020		
	Area (km^2)	Number	Mass Balance (m w.e.a^{-1})	Area (km^2)	Number	Mass Balance (m w.e.a^{-1})
Lake-terminating glaciers	70.29±2.69	46	-0.36±0.26	49.6±1.82	34	-0.56 ±0.31
Debris-covered glaciers	55.42±1.25	5	-0.20±0.34	51.59±1.77	5	-0.44 ±0.47

Debris-covered and lake-terminating glaciers	5.46±0.32	1	-0.18±0.80	6.05±0.32	1	-0.34±0.92
Regular glaciers	615.29±20.73	617	-0.30±0.10	554.64±22.93	692	-0.42±0.12

663

Figure captions

Figure 1 (a) Overview of study area. (b) Glaciers distribution. Label I in the large, red dotted rectangle represents the SW section of the WNR and Label II in the small, dark red dotted rectangle represents the NE section.

Figure 2 Glacier distribution in the WNR in 1976, 2000, 2009, 2014 and 2020. (a) Number and area of glaciers by size category. (b) Distribution of glacier area with altitude. (c) Distribution of glacier area with slope. (d) Distribution of glacier area with aspect. Data in 2009 came from Chinese Glacier Inventory II.

Figure 3 The distribution of glacier area change in the WNR from (a) 1976 to 2000, (b) from 2000 to2020, (c) 1976 to 2020.

Figure 4 Glacier area changes with (a) time, (b) elevation, (c) slope and (d) aspect. The short lines on either side of the point indicate the margin of error in figure (a, b, c).

Figure 5 Mean annual glacier surface elevation changes in the WNR from (a) 1976 to 2000, (b) 2000 to 2020, and (c) 1976-2020. Label I in (a, b, c) represents the SW section and label II in (b) represents the NE section of the WNR (on the same scale). The red rectangular box in (b) shows an area of the centra WNR referred to in the paper.

Figure 6 Glacier elevation change with altitude (m a.s.l) in the whole WNR, inside Nam Co drainage basin and outside Nam Co drainage basin from (a) 1976 to 2000 and (b) 2000 to 2020. The dots represent the mean elevation change in each 50-m elevation bin and shaded regions in the altitudinal distributions indicate the uncertainty.

Figure 7 The distribution of glacier-wide mass balance for individual glaciers (> 2 km^2) in the WNR from (a) 1976 to 2000, and (b) from 2000 to2020. Label I represents the SW section and label II represents the NE section of the WNR (on the same map scale).

Figure 8 Glacier elevation change from 1976 to 2000 and from 2000 to 2020 with (a) elevation, (b) slope, and (c) aspect. The dots in figure (a) represent the mean elevation change in each 50-m bin and shaded region in (a) indicate the uncertainty in the altitudinal distributions. (b) is boxplot of dh in 2-° slope bins and four lines from bottom to top for one box represent minimum value, 25th percentile, 75th percentile, and maximum value, respectively and dots in figure (c) represent the mean elevation change in each 2-° slope bin. (c) represent the mean elevation change in each 45-°aspect bin.

Figure 9 Glacier area changes with slope during 1976-2000 (a) and during 2000-2020 (b), and glacier elevation changes with slope during 1976-2000 (c) and during 2000-2020 (d).

Figure 10   Rate of glacier elevation change with elevation of different glaciers types during (a) 1976-2000 and (b) 2000-2020. Plots represent the mean values of glacier elevation change in each 50-m elevation bin and shaded regions indicate the uncertainty in the altitudinal distributions.

Figure 11   (a) Glacier elevation change in the WNR during 2000-2014. (b) Glacier elevation changes with altitude in the WNR, inside Nam Co drainage basin and outside Nam Co drainage basin from 2000 to 2014. The dots represent the mean elevation change in each 50-m elevation bin and shaded regions indicate the uncertainty in the altitudinal distributions. (c) Total area of glaciers and that area covered by the datasets during 1976-2000 and 2000-2014.

Figure 12   Temperature and precipitation changes for the study area at Damxung, Lhasa and Bange stations from 1976 to 2020. Annual average temperature and precipitation (a, b), ablation season (June to September) average temperature and precipitation (c, d), accumulation season (January to May and October to December) average temperature and precipitation (e, f).

Figure 13   Gridded temperature and precipitation change during specific time periods.

Figure 1   (a) Overview of study area. (b) Glaciers distribution. Label I in the large, red dotted rectangle represents the SW section of the WNR and Label II in the small, dark red dotted rectangle represents the NE section.

705

706 Figure 2   Glacier distribution in the WNR in 1976, 2000, 2009, 2014 and 2020. (a) Number and area of glaciers by size

707 category. (b) Distribution of glacier area with altitude. (c) Distribution of glacier area with different slope. (d) Distribution of

708 glacier area with aspect. Data in 2009 came from Chinese Glacier Inventory II.

709
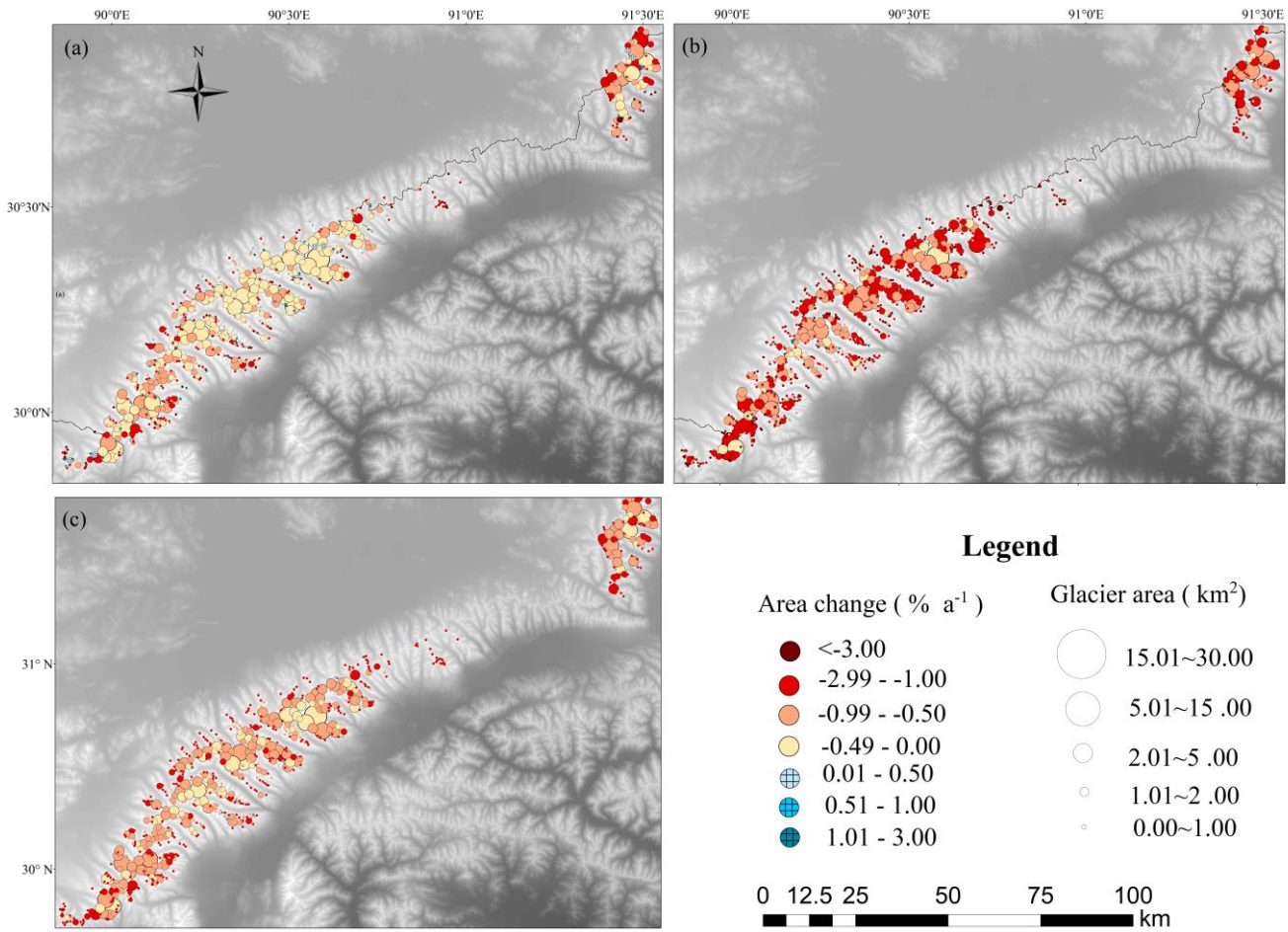
710
711 Figure 3   The distribution of glacier area change in the WNR from (a) 1976 to 2000, (b) from 2000 to2020, (c) 1976 to
712 2020.
713
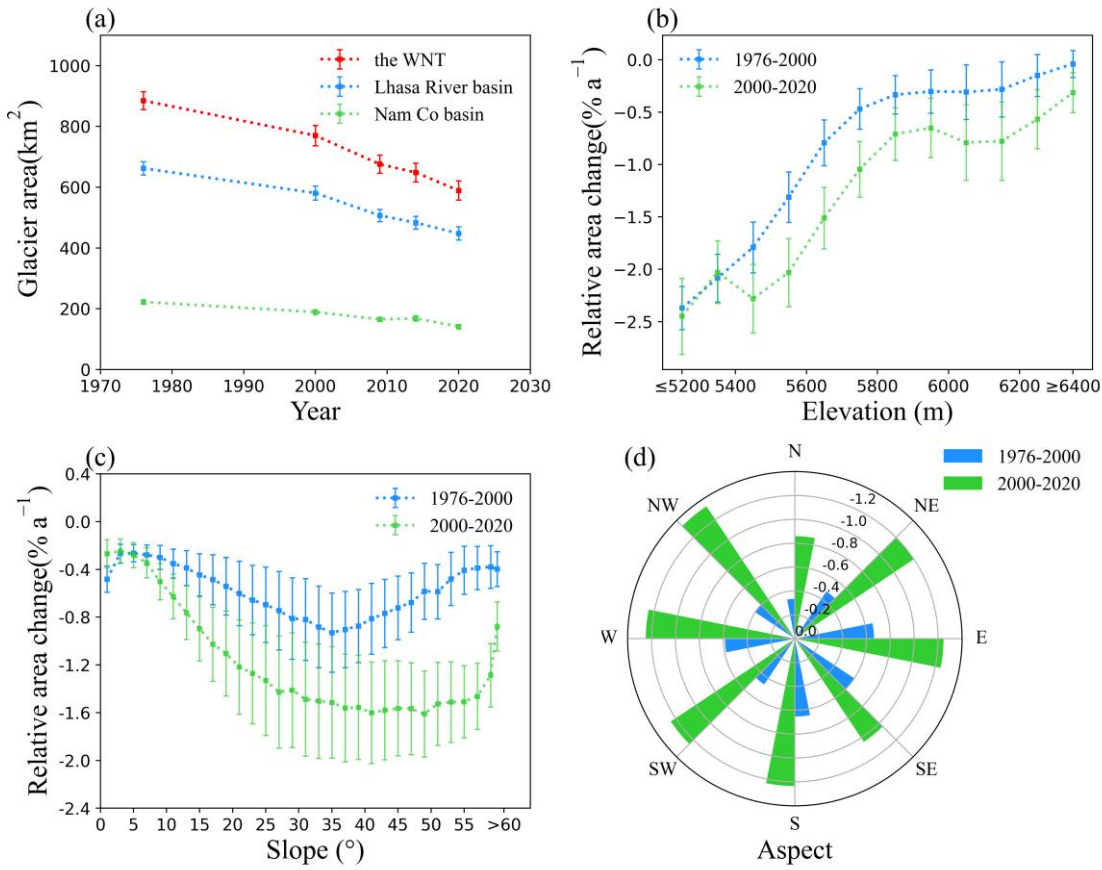
714

715   Figure 4   Glacier area changes with (a) time, (b) elevation, (c) slope and (d) aspect. The short lines on either side of the point

716   indicate the margin of error in figure (a, b, c).
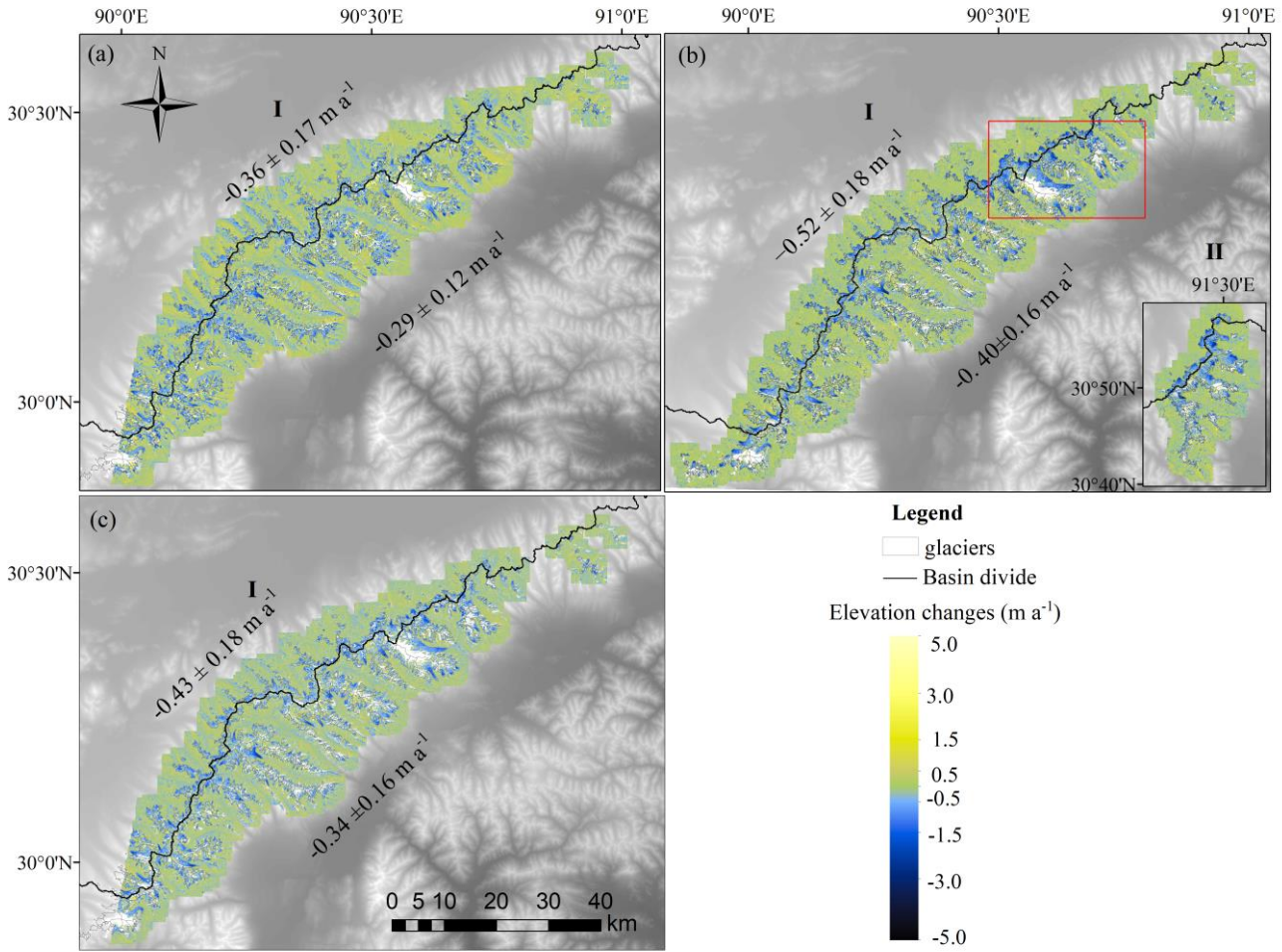
717

718   Figure 5   Mean annual glacier surface elevation changes in the WNR from (a) 1976 to 2000, (b) 2000 to 2020, and (c)

719   1976-2020. Label I in (a, b, c) represents the SW section and label II in (b) represents the NE section of the WNR (on

720   the same scale). The red rectangular box in (b) shows an area of the centra WNR referred to in the paper.
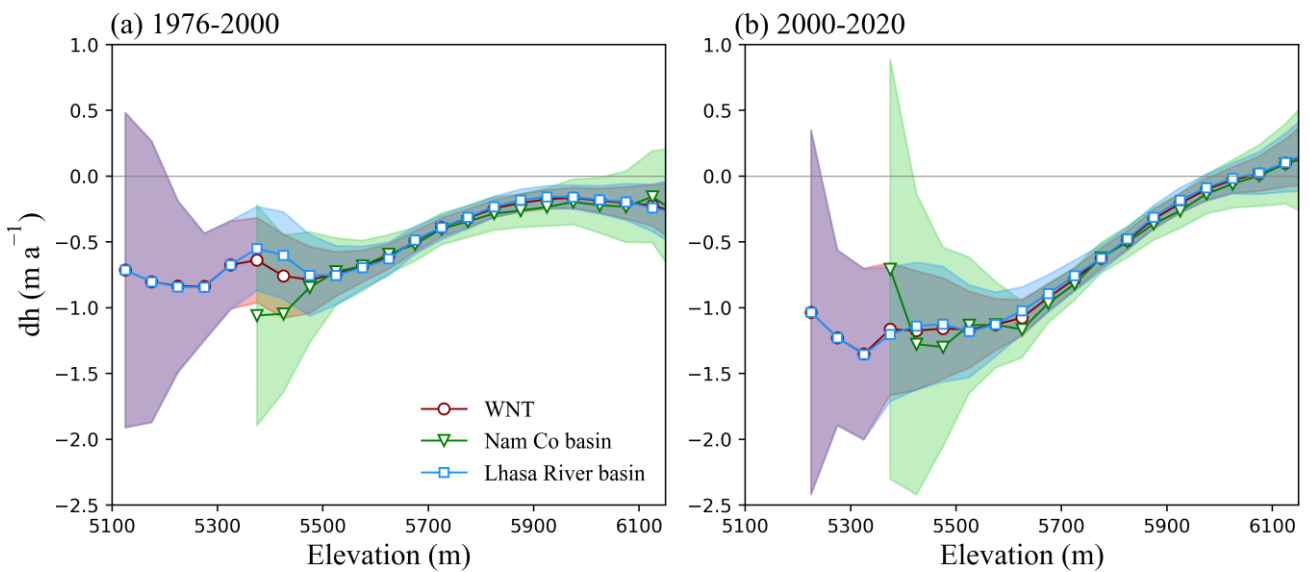
721

722 Figure 6   Glacier elevation changes in relation to elevation (m a.s.l) in the whole WNR, inside Nam Co drainage basin and

723   outside Nam Co drainage basin from (a) 1976 to 2000 and (b) 2000 to 2020 (b). The dots represent the mean elevation change

724   in each 50-m elevation bin and shaded regions in the altitudinal distributions indicate the uncertainty.
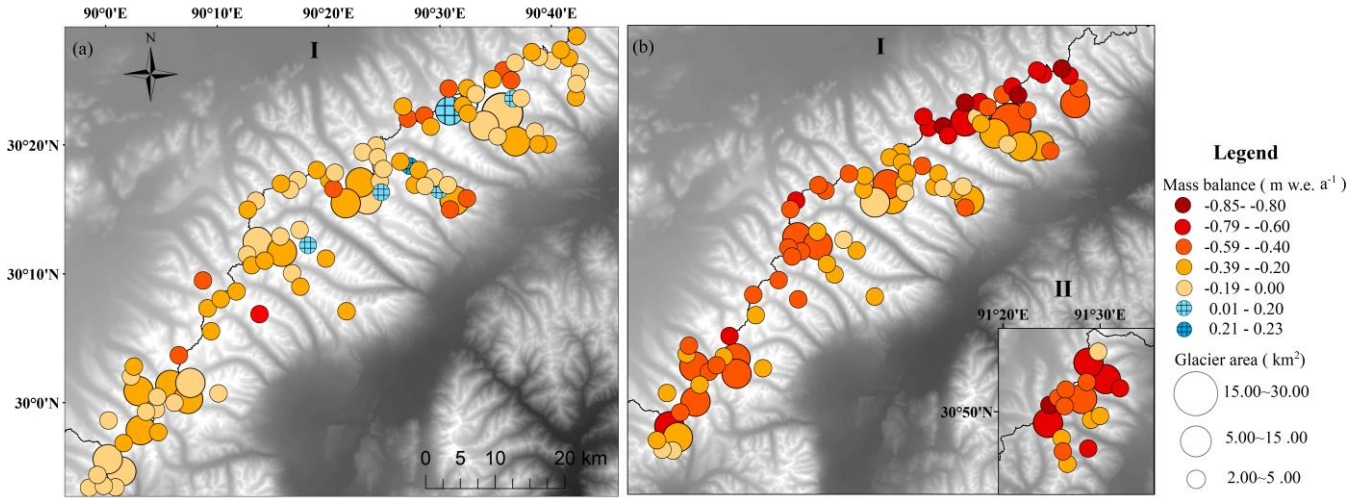
725

726 Figure 7   The distribution of glacier-wide mass balance for individual glaciers (> 2 km^2) in the WNR from (a) 1976 to 2000

727   and (b) 2000 to2020. Label I represents the SW section and label II represents the NE section of the WNR (on the same map

728   scale).
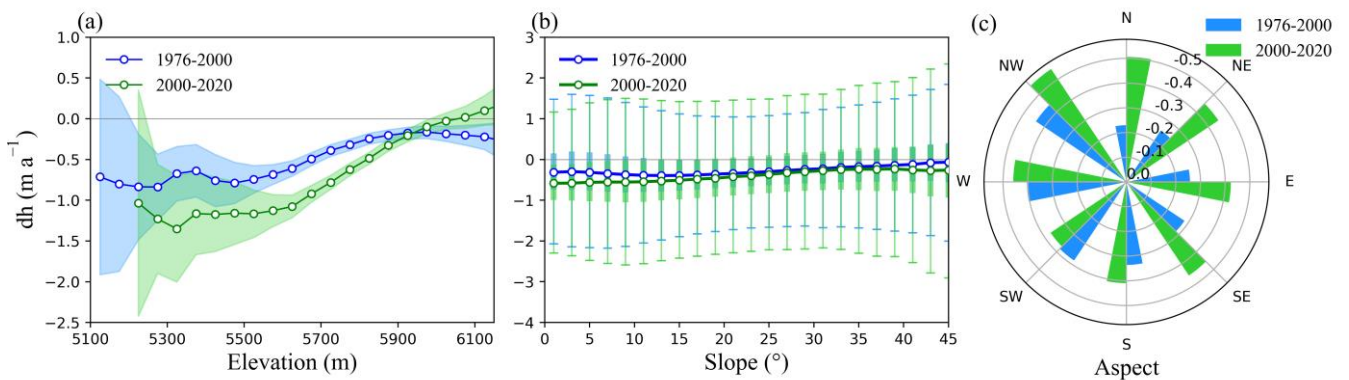
729

730 Figure 8   Glacier elevation changes from 1976 to 2000 and from 2000 to2020 with (a) elevation, (b) slope and (c) aspect. The

731   dots in figure (a) represent the mean elevation change in each 50-m bin and shaded region in (a) indicate the uncertainty in the

732   altitudinal distributions. (b) is boxplot of dh in 2-° slope bins and four lines from bottom to top for one box represent minimum

733   value, 25th percentile, 75th percentile, and maximum value, respectively and dots in figure (c) represent the mean elevation

734   change in each 2-° slope bin. (c) represent the mean elevation change in each 45-°aspect bin.
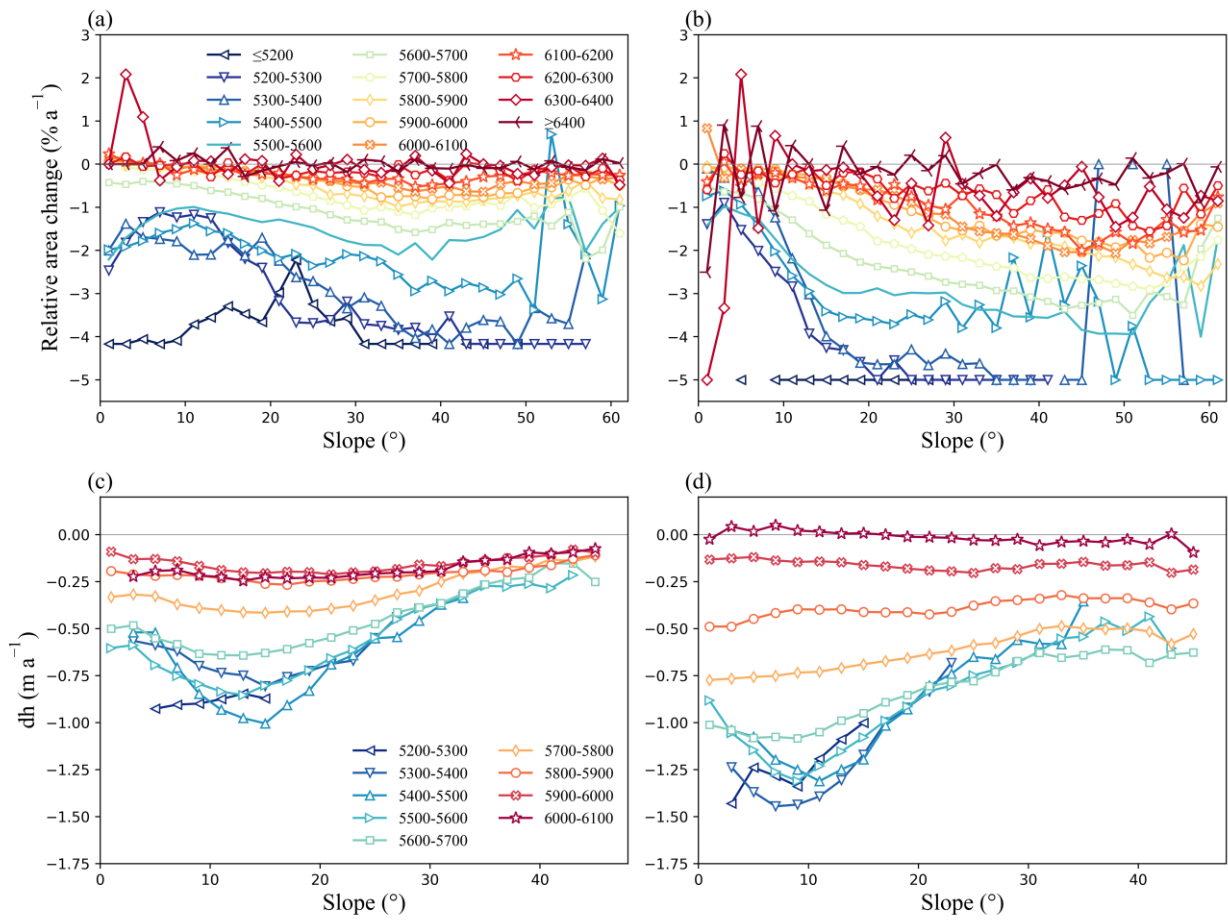
Figure 9 Glacier area changes with slope during 1976-2000 (a) and during 2000-2020 (b), and glacier elevation changes with slope during 1976-2000 (c) and during 2000-2020 (d).
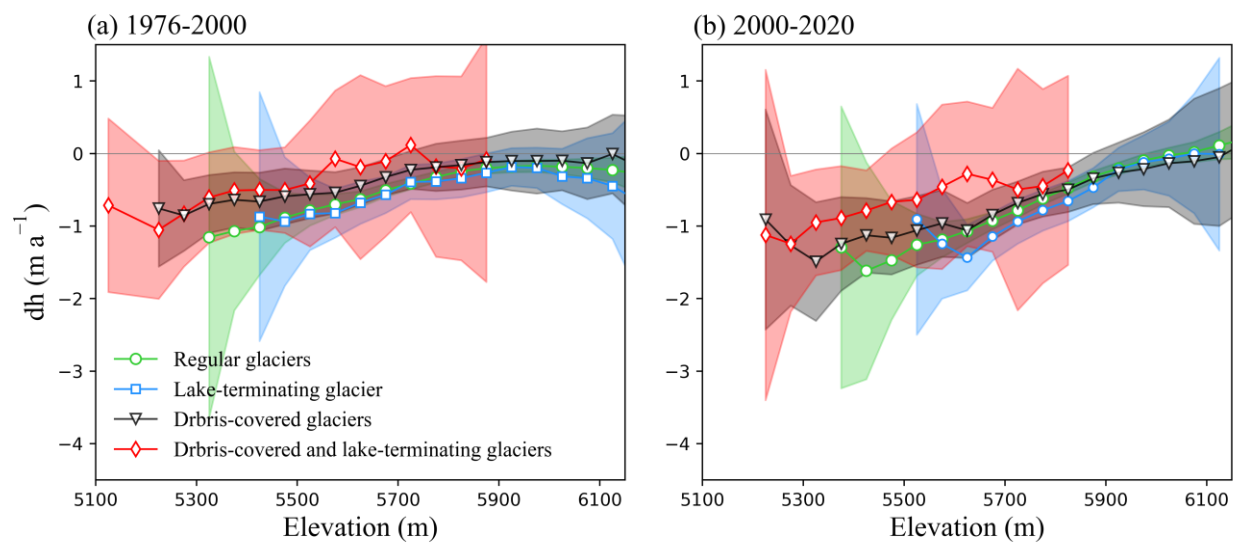
Figure 10 Rate of glacier elevation change with elevation of different type glaciers during (a) 1976-2000 and (b) 2000-2020 (b). Plots represent the mean values of glacier elevation change in each 50-m elevation bin and shaded regions indicate the uncertainty in the altitudinal distributions.
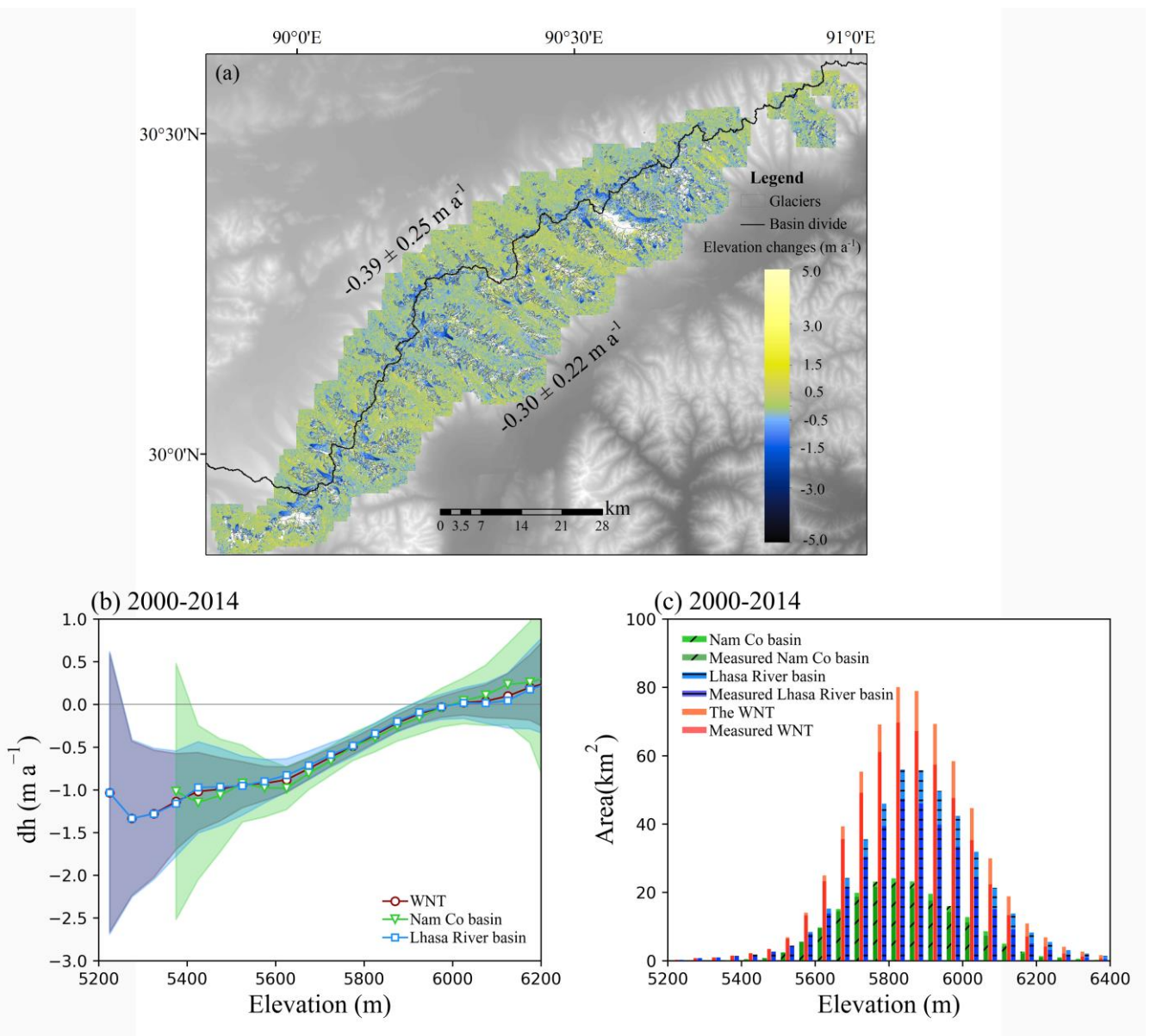
Figure 11   (a) Glacier elevation change in the WNR during 2000-2014. (b) Glacier elevation changes in relation to elevation with altitude in the WNR, inside Nam Co drainage basin and outside Nam Co drainage basin from 2000 to 2014. The dots represent the mean elevation change in each 50-m elevation bin and shaded regions indicate the uncertainty in the altitudinal distributions. (c) Total area of glaciers and that area covered by the datasets during 1976-2000 and 2000-2014.
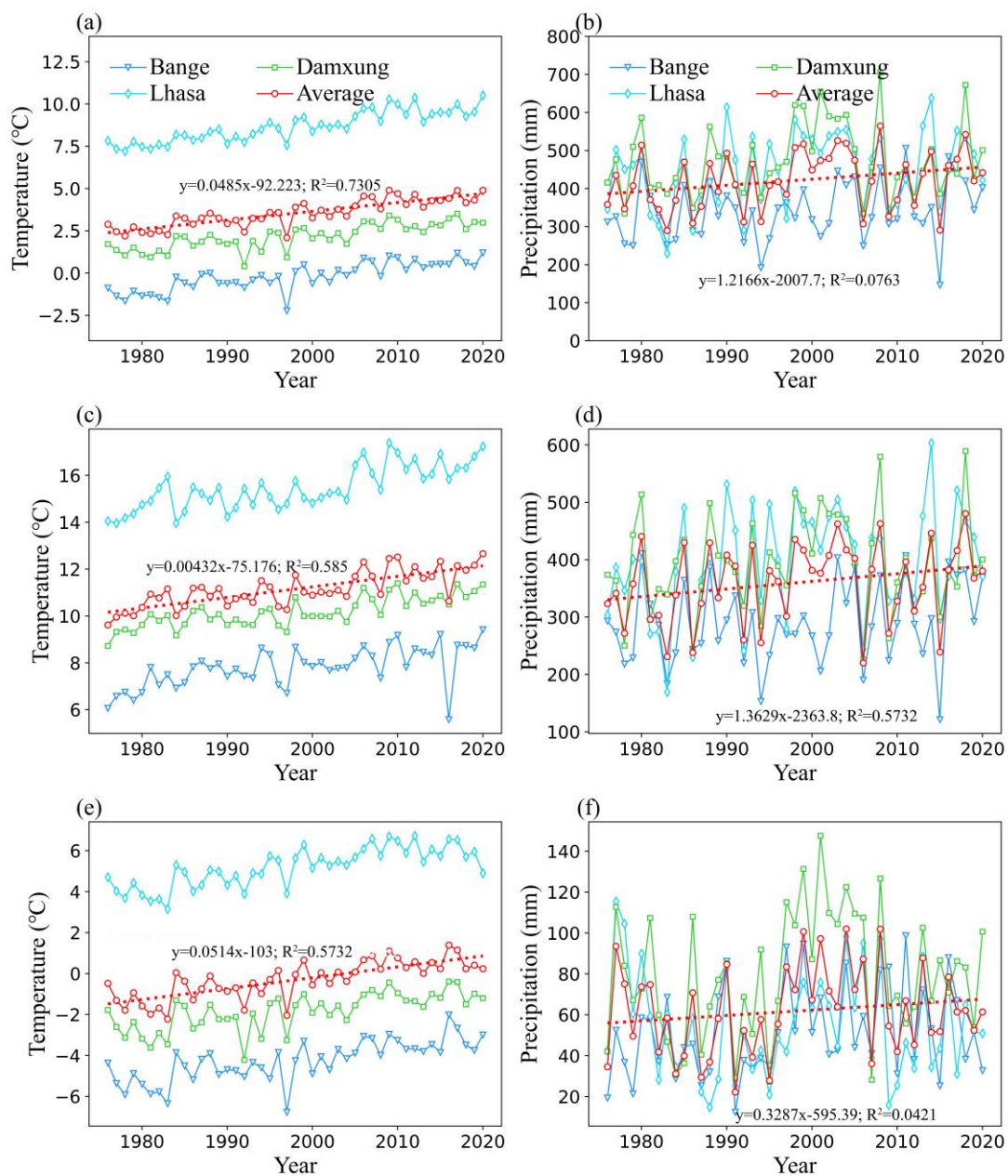
748

749   Figure 12   Temperature and precipitation changes for the study area at Damxung, Lhasa and Bange stations from1976 to

750   2020. Annual average temperature and precipitation (a, b), ablation season (June to September) average temperature and

751   precipitation (c, d), accumulation season (January to May and October to December) average temperature and precipitation (e,

752   f).

753

754
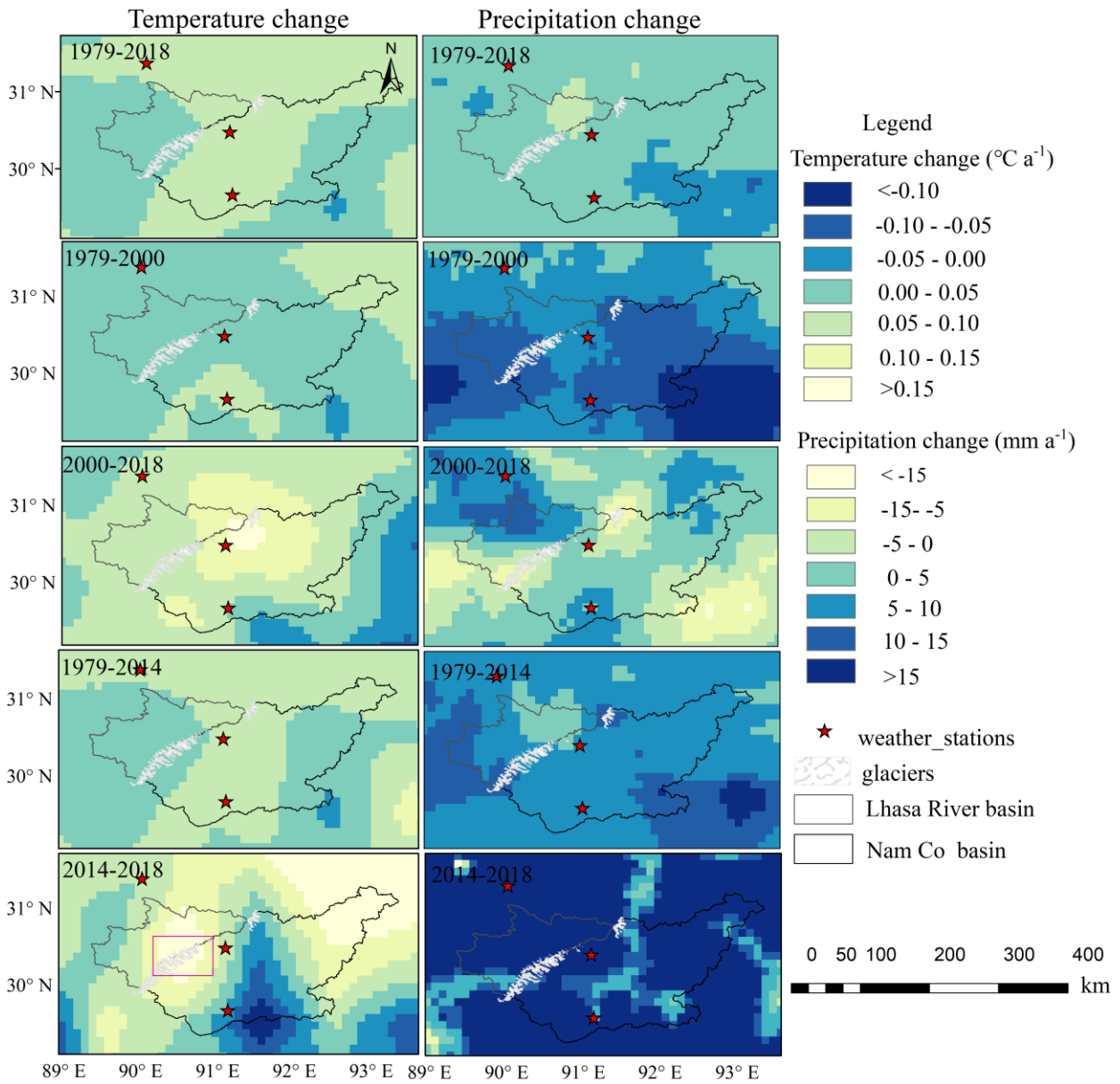
755

756   Figure 13   Gridded temperature and precipitation change during specific time periods.